PRO-AROMATIC DYE COMPONENTS FOR DYE-SENSITIZED SOLAR CELLS: THIENOTHIOPHENE AND INDOLIZINE

by
George Andrew Puneky

A thesis submitted to the faculty of The University of Mississippi in partial fulfillment of the requirements of the Sally McDonnell Barksdale Honors College

Oxford
May 2015

Approved by

_____
Advisor: Professor Jared Delcamp

_____
Reader: Professor Davita Watkins

_____
Reader: Professor Jason Ritchie

ACKNOWLEDGEMESNTS

We thank the Mississippi NSF-EPSCOR program (EPS-0903787), the University of Mississippi, and the UM Sally McDonnell Barksdale Honors College for funding this project. In addition, G.A.P would like to thank Dr. Jared Delcamp and the team of undergraduate and graduate researchers involved with the Delcamp Group for their continued support and guidance toward completion of this project.

ABSTRACT

Four D-π-A dyes based on a 3,4-thienothiophene π-bridge were synthesized for use in dye-sensitized solar cells (DSCs). The pro-aromatic building block 3,4-thienothiophene has been reported to stabilize dye excited-state oxidation potentials. This lowering of excited-state energy levels permits for increased absorption into the near-infrared (NIR) region using relatively low molecular weight dyes. Strong donor functionality based on triaryl- and diarylamines are employed in the dye designs to raise both the ground and excited-state oxidation potentials to values capable of generating DSC devices with good open-circuit voltages. Solubility, aggregation, and TiO_2 surface protection were addressed by examining an ethylhexyl alkyl chain in comparison to a basic ethyl chain on the thienothiophene bridge. Through this minor structural modification, a drastic increase in overall efficiency of up to 7.8% is observed. Again in an attempt to stabilize dye excited-state oxidation potentials through competing local aromaticity, a fifth dye was synthesized to incorporate a pro-aromatic indolizine-based donor moiety. Preliminary optical and electrochemical results with regards to the indolizine-based dye appear to be undesirable in terms of prospective cell performance. These preliminary results are believed to stem from the excessively strong electron withdrawing tricyanofuran acceptor unit seen in this dye.

TABLE OF CONTENTS

Introduction.

Since the dawn of the Industrial Revolution society has evolved with the vague assumption that mankind would always have access to a sufficient supply of energy resources. The vast majority of consumed energy in the world is generated by three fossil fuels: natural gas, coal, and petroleum. Other major sources of energy being exploited in modern day consist of nuclear power and renewable energy (hydroelectric, wind, solar). The distribution of energy consumption by source in the United States is illustrated in *Figure 1*.

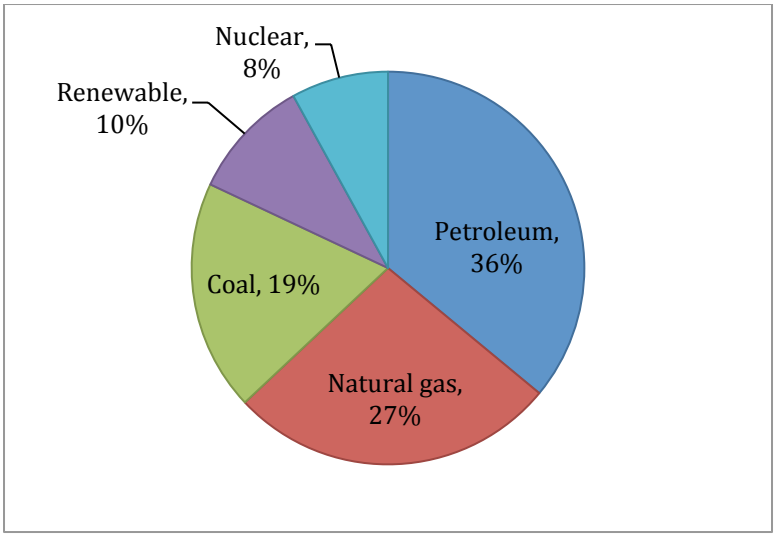

Figure 1. United States distribution of energy consumption.[1]

The lifestyle of present day society has reached a point at which the community is completely dependent on fossil fuels, an energy source that will in fact eventually "run out". One cannot begin to imagine the catastrophe that would arise if one day we were to wake up without these highly coveted resources. Based on the known fossil fuel reserves in the world, experts have suggested that all known crude oil and natural gas will be

extracted roughly within the next 50 years, while coal mining will persist for 100 years or more.[2] This dark foreshadowing of a near future deprived of energy has set the stage for present day science to develop various solutions.

At the current state of scientific knowledge, solar energy is the clear frontrunner in the race to power the future. Although there are multiple reasons why the potential of solar energy trumps the broadly used fossil fuels of today, such as labor and pollution, it is essentially a futile argument in the sense that these fossil fuels will soon be non-existent. A renewable source of energy is needed. Among the forms of renewable energy, solar energy possesses an impressive resume in light of others such as hydroelectric and wind. Hydroelectric power generally relies on the use of large-scale dams that carry a very expensive price tag and give rise to possible geological damage and negative effects on wildlife. In light of the already mentioned downfalls of hydroelectric power, the most important deterrent of its use is the fact that the production of hydroelectric power has reached near capacity, with little room for growth.[3] Wind energy also has its associated cons such as turbine maintenance, region specific noise, and the requirement of large areas of land.[3] Solar energy stands as a solution to virtually all problems associated with other forms of renewable energy. Solar panels require essentially no maintenance and do not cause environmental damage or pollution. Costs associated with the installation of solar panels may not be inexpensive initially, but the accumulation of electricity savings will soon surmount to pay for the initial investment. Unlike water and wind, sunlight can be found nearly anywhere on earth.[3] Given this, and the fact that solar panels are easily installed on existing unused space such as rooftops, the option of solar energy is very versatile.

Solar cells that are commercially available today are primarily composed of fairly expensive inorganic silicon semiconductors. The use of organic solar cells appears to be a cost efficient alternative to the presently used silicon-based solar cells. Dye-sensitized solar cells (DSCs) have recently attracted much attention as a promising future technology implementing an organic-based solar cell design. Functional ruthenium-based complexes, zinc-porphyrins, and metal free organic donor-acceptor systems are the three main classes of dye sensitizers currently used in DSC. Ruthenium-based dyes have been show to produce impressive efficiencies, but at a high expense and associated risks in difficult synthesis and purification, while zinc-porphyrin dyes have been associated with a limited light harvesting range.[5] The alternative class of metal free organic dyes are currently at a developmental state of slightly lower efficiency but provide a promising future outlook in their low expense, tunable and easily synthesized molecular structures, and typically higher molar extinction coefficients compared to that of their competitors.[6] *Figure 2* illustrates a typical donor-π-bridge-acceptor (D-π-A) structural design for metal free organic dyes, along with electron transfer arrows that are further detailed in *Figure 3*.

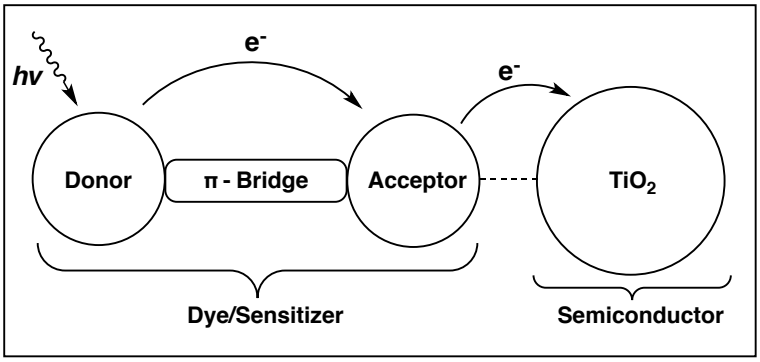

Figure 2. Organic D-π-A dye design illustrating the pathway of electron injection.[4]

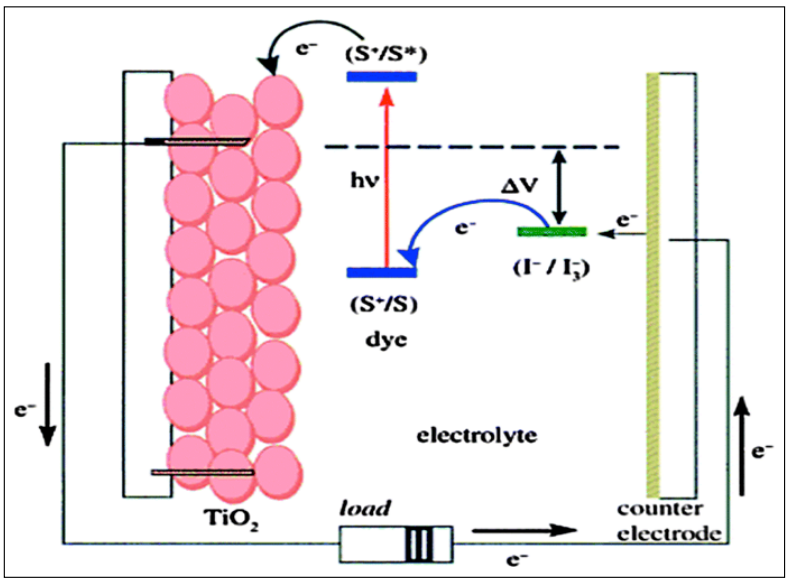

Figure 3. DSC schematic illustrating the general working mechanism of the cell.[7]

Figure 3 illustrates a DSC schematic and the basic pathways necessary to the device's function. Initial photon absorption by the dye-sensitizer induces electron excitation from the ground-state (S^+/S) to the excited-state (S^+/S^*). The excited-state electron is then injected into the conduction band of a metal oxide electrode (TiO_2). After injection, the electron is conducted to the anode and then travels via an external connection to the cathode counter electrode. Reduction of the redox couple (commonly I^-/I_3^-)[9] takes place at the cathode and is used to complete the circuit upon electron donation to regenerate the ground-state dye.[6]

The main parameter of interest in the process illustrated in *Figure 3* is the photon conversion efficiency (η, PCE), which represents how efficiently sunlight is converted to usable electrical energy. PCE is determined to be the product of the short circuit current (J_{SC}), the open circuit voltage (V_{OC}), and the fill factor (FF).

$$\eta = J_{sc}V_{oc}FF$$

Equation 1. PCE equation.

The maximum J_{SC} is relative to how much light can be absorbed by the sensitizer, while the maximum V_{OC} is a measurement of the potential difference between the conduction band of the metal oxide and the valence band of the redox couple. *FF* is a variable that is largely dependent on the internal resistance present in the device.

In order to develop a highly efficient cell, all thermodynamic and kinetic parameters must be accounted for with regards to dye structure. An energetically favorable driving force is necessary for electron injection (ΔG_{inj}) from the excited-state sensitizer into the metal oxide conduction band as well as a favorable driving force for the regeneration of the ground-state sensitizer (ΔG_{reg}). It is noted that a minimal driving force of ~200 mV is needed for an efficient injection and regeneration event.[6] If these driving forces are not sufficient, counter-productive alternate electron transfer pathways can emerge. The main interfering pathways of concern consist of: photorelaxation of excited-state electrons back to the ground-state, unfavorable direct electron transfer between the metal oxide and sensitizer (the "back-reaction"), and unfavorable cyclical electron transfer between the metal oxide and redox shuttle (recombination). Common dye structural features incorporated to correct these potential issues are positioning of the high electron affinity donor subunit far away from the metal oxide surface in order to slow the back-reaction, and the implementation of long alkyl chains to block communication between the redox couple and metal oxide, thus diminishing recombination.

With fossil fuel resources quickly fading, a new source of energy will be required to fill the gap left by the world's soon-to-be depleted oil reserves. Since the introduction of DSCs in 1991,[8] tremendous efforts have been made to bring this new technology to the forefront of alternative energy options.[6] For the major part of the past two decades, devices using ruthenium-based sensitizers have dominated the DSC field, possessing the best electronic parameters and providing cells of the highest efficiency.[10, 11, 12, 13] For the first time in 2014, a purely organic dye, **ADEKA-1**,[14] and a porphyrin-based dye, **SM315**,[15] were seen to surpass these ruthenium-based dyes with PCEs of 12.5% and 13.0% respectively. The success of these dyes are largely driven by the iterative use of ubiquitous, modular D-π-A dye design. As previously mentioned, dyes of this nature are typically much more cost efficient as they do not rely on expensive metals and commonly make use of straightforward synthetic schemes. PCE improvements over these impressive devices is reasonable and would be aided through the careful development of building blocks allowing tunable access to the near-infrared (NIR, ~750 nm) region of the solar spectrum.[10] Pro-aromatic building blocks are promising dye components that allow for tunability into the NIR region using dyes of relatively low molecular weights.

Certain sensitizers have incorporated the use of pro-aromatic structures.[15,16,17] These structures benefit from an increase in stability provided by an area of local aromaticity present in their excited-state. This phenomenon is illustrated with a comparison of **L1** with that of **DP1** in *Figure 4*. As a result of pro-aromatic excited state stabilization, photoexcitation occurs at significantly lower photonic energies, whereas the ground state energy level is relatively unaffected leading to a narrowing of the optical band gap.

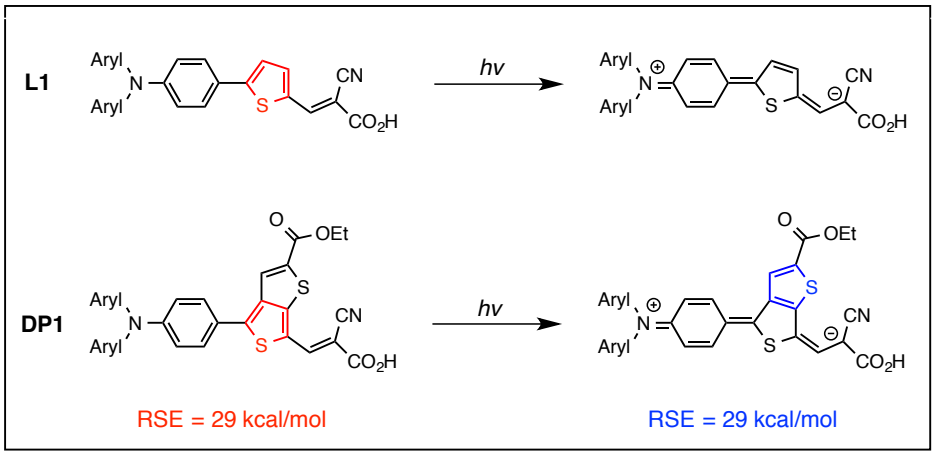

Figure 4. A comparison of a D-π-A dye designed using a common aromatic building block (such as **L1**[18]) with a dye containing a pro-aromatic building block (**DP1**) leading to competing local aromaticity in the ground state and excited state of the dye. Local resonance stabilization energies of these π-bridges in their ground and excited-states are illustrated.

In 2012, Chen, et. al.[17] synthesized a series of dyes incorporating a pro-aromatic conjugated building block, 3,4-thienothiophene (3,4-TT), as a π-bridge. Ten dyes in total were designed around this structure with the highest PCE reaching 5.3% (**MCT-1**). Regardless of the incorporation of the 3,4-TT pro-aromatic structure, these dyes were found to suffer from relatively poor V_{OC} values stemming from low excited-state oxidation potentials ($E_{(S+/S*)}$), requiring the addition of excessive lithium (lithium doping) in order to artificially lower the TiO_2 conduction band to boost ΔG_{inj} values. We believe that by making minor alterations to the dye structure, electrochemical parameters can be improved, thereby increasing the overall PCE values. Coarse tuning of $E_{(S+/S*)}$ values may be accomplished through the selection of electron deficient functionality; however,

$E_{(S+/S^*)}$ values may be finely tuned through donor building block selection. Increasing electron donating strength leads to a weak destabilization of the dye $E_{(S+/S^*)}$ values. To evaluate this claim, we have synthesized a series of dyes analogous to the **MCT-1** structure. Alterations to the original **MCT-1** structure include: increasing the strength of the triphenylamine (TPA) donor via installation of hexyloxy chains (**DP1**, **PB1**), as well as using a stronger indoline-based donor (**DP2**, **PB2**). In addition to altering donor strength, in **PB1** and **PB2**, we have installed an ethylhexyl ester to 3,4-TT as an attempt to reduce any possible aggregating issues and to improve dye solubility. *Figure 5* illustrates the structures of **MCT-1**, **DP1**, **DP2**, **PB1**, and **PB2**.

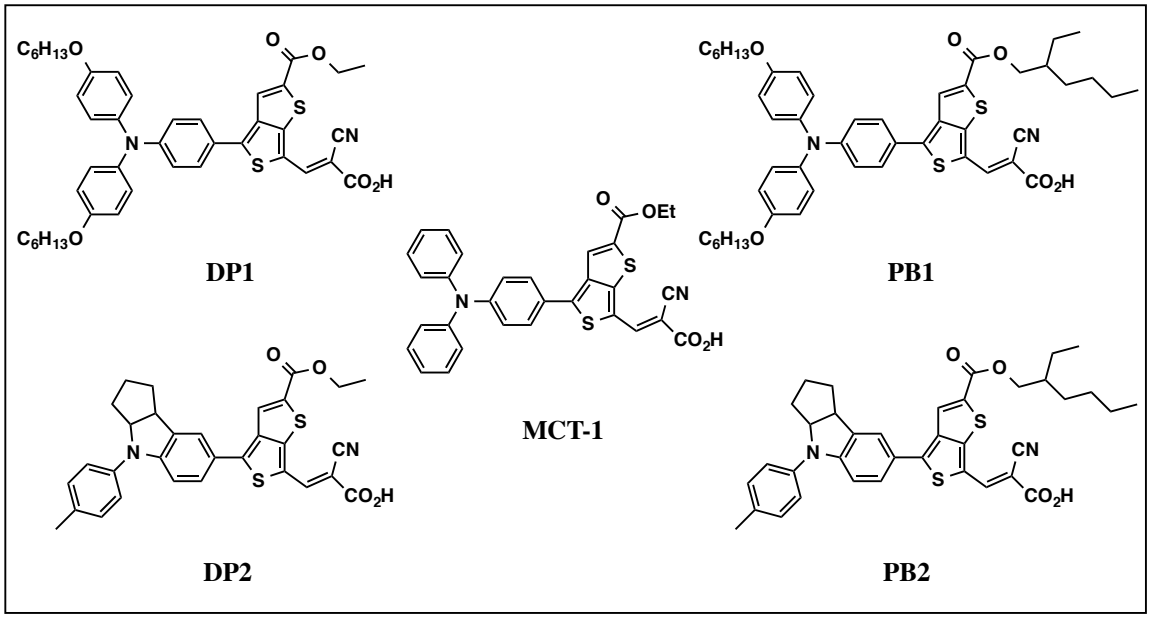

Figure 5. Structural comparison of **MCT-1**, **DP1**, **DP2**, **PB1**, and **PB2**.

In addition to 3,4-TT, we have synthesized a novel pro-aromatic indolizine-based donor system for use in DSC dyes. Pro-aromatic structures are rare in donor functionality and are more commonly seen in π-bridge and acceptor subunits. *Figure 6* illustrates dye

DP3 that was synthesized to incorporate an indolizine-based donor. This figure also shows the pro-aromatic excited-state stabilization of the indolizine-based donor system.

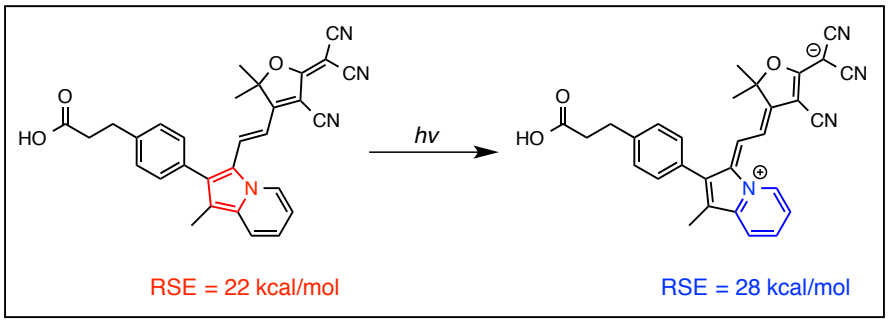

Figure 6. Competing local aromaticity observed in a dye incorporating an indolizine-based pro-aromatic structure (**DP3**) leading to excited-state stabilization. Local resonance stabilization energies are noted.

We believe this novel donor system will improve upon presently used donor moieties as a result of the reduction in the charge transfer energy barrier between the ground- and excited-states present in indolizine. In addition to the incorporation of an indolizine-based donor, **DP3** also makes use of a very strong tricyanofuran (TCF) acceptor subunit and a lateral chain propanoic acid anchoring group for attachment to the surface of the TiO_2 semiconductor. This type of anchoring group was first used by Hao et, al.[19] in 2009 in order to allow for fine-tuning of the acceptor subunit, above that of the limited tuning possibilities seen in the commonly used cyanoacrylic acid acceptor.

HY103, synthesized by Hao et, al.,[19] is used in comparison to **DP3** in order to assess the performance of the indolizine donor system due to the identical nature of the acceptor and anchoring groups seen in these dyes (*Figure 7*).

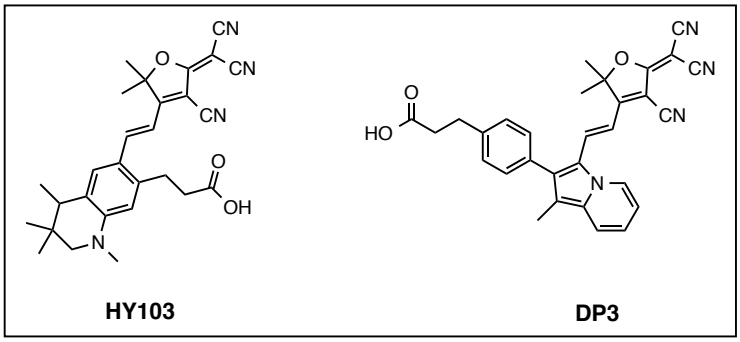

Figure 7. Structural comparison of **DP3** and **HY103**.

Results and Discussion: Thienothiophene.

Synthesis: DP1, DP2, PB1, and PB2

The synthesis of the **DP** and **PB** TT-series proceeds in 6-synthetic steps according to *Scheme 1*. Lithium halogen exchange with commercially available 3,4-dibromothiophene and quenching with DMF leads to bromoaldehyde **1**. A one-pot Cu-catalyzed thiol cross-coupling and condensation reaction was employed to form the 3,4-TT ester **2**. The subsequent Vilsmeier-Haack reaction on **2** yields two regioisomers **3a** and **3b** (in a 1:2 mixture) which vary by orientation of the proaromatic ring sulfur on the opposite (**3a**) or same side (**3b**) as the aldehyde. The desired isomer, **3b,** undergoes NBS bromination to give the bromoaldehyde **4** in 4-steps and 18% overall yield. Arylamine donor building blocks were installed through Suzuki coupling reactions to give intermediate **5**. Dyes **DP1, DP2, PB1** and **PB2** were completed through Knoevenagel condensation with cyanoacetic acid (CAA) to give the final dyes (**6)** in 6 linear steps from commercial starting materials and up to ~13% overall yield.

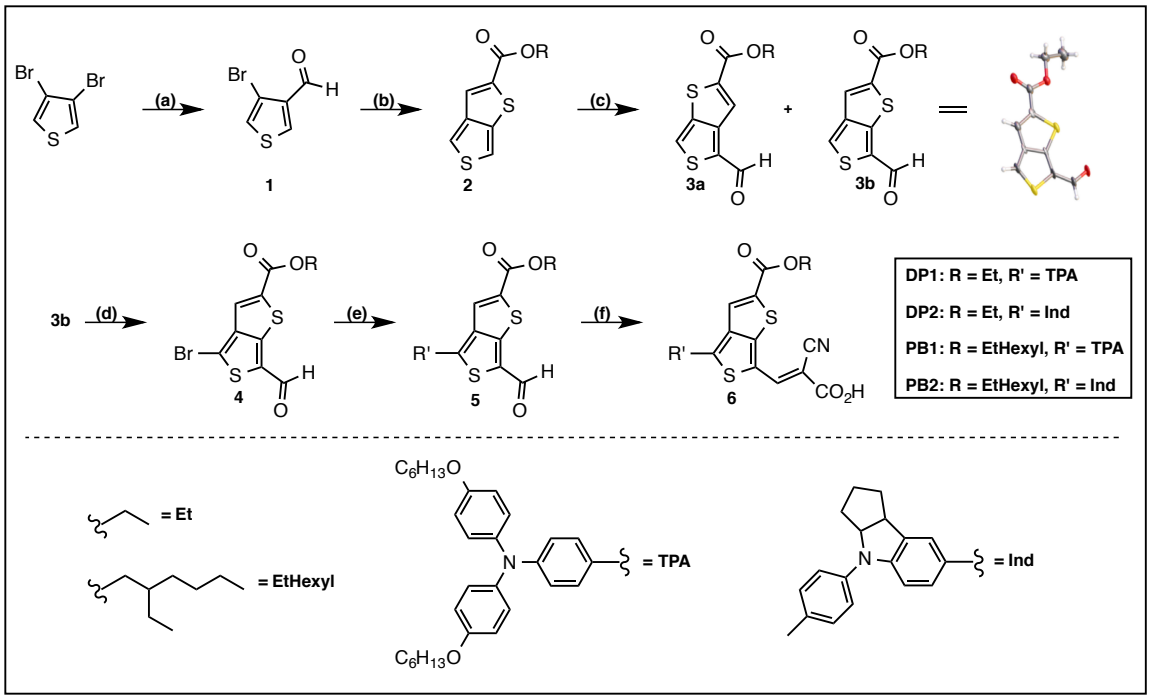

Scheme 1. Synthetic scheme for dyes **DP1**, **DP2**, **PB1**, and **PB2**. (a) i. t-BuLi (1.5 equiv.), 0.8 M Et_2O, -78^{0}C, 30 min; ii. DMF (1.1 equiv.), -78^{0}C to r.t., 4 hr; 30%. (b) ethyl mercaptoacetate (or ethylhexyl mercaptoacetate, 1.1 equiv.), CuO (3%), K_2CO_3 (1.5 equiv.), 0.5 M DMSO, 60^{0}C, 16 hr; 56% (EtHexyl); 80% (Et). (c) i. $POCl_3$ (1.3 equiv.), DMF (1.3 equiv.), 0.4M DCE, 0^{0}C, 2.5 hr; ii. 0.4 M KOH (1.0 M, aq), r.t., 15 min; 48% (EtHexyl); 71% (Et). (d) NBS (1.5 equiv.), 0.2 M DMF, 0^{0}C to r.t., 24 hours; 62% (EtHexyl); 82% (Et). (e) TPA-Bpin (or Ind-Bpin, 1.1 equiv.), K_3PO_4 (3.0 equiv.), Pd_2dba_3 (4%), X-Phos (16%), 0.05 M toluene, 1.1 M H_2O, 80^{0}C, 6 hr; 75% (TPA-EtHexyl); 93% (TPA-Et); 84% (Ind-EtHexyl); 26% (Ind-Et). (f) cyanoacetic acid (3.0 equiv.), piperidine (7.0 equiv.), 0.06 M $CHCl_3$, 90^{0}C; 48%.

^{1}H NMR of isomers **3a** and **3b** yield three singlets in the aromatic region with only slight shifts in ppm values for each isomer. NOE NMR and X-ray crystallography techniques were employed to unambiguously assign the correct structure to these isomers. A slight NOE response is observed between the aldehyde-H and proaromatic thiophene-H for isomer **3a** with no NOE response observed for any of the hydrogens in **3b** (*Figure 8*). X-ray quality crystals were obtained from isomer **3b** through the use of vapor infusion of hexanes into a solution of **3b** in toluene to give long yellow needles. The NOE NMR results and X-ray crystallography results both confirm **3b** as the desired isomer, which was formed as the major product. Aldehydes **3a** and **3b** are separable on silica gel chromatography with **3b** having a slightly lower R_f value. This regioselective route proved reliably scalable to multiple gram batches of isomer **3b**.

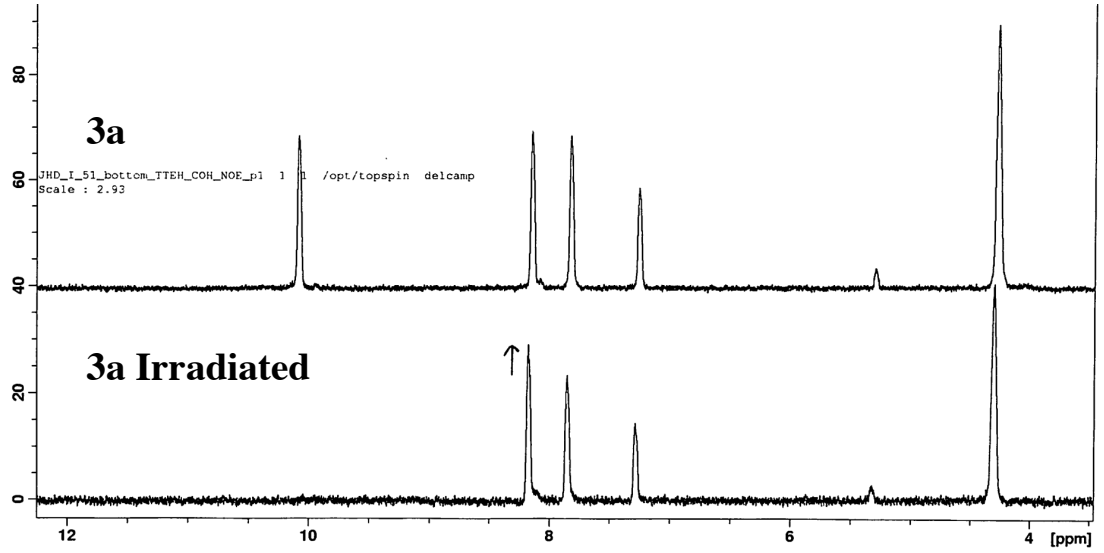

Figure 8. NOE NMR spectrum of intermediate **3a** with irradiated aldehyde-H.

Optical and electrochemical properties

Making minor design modifications to the **MCT-1** structure produced considerable effects on the optical and electrochemical dye parameters. This information is summarized in *Table 1*. Via attachment of two donating hexyloxy chains to the triphenylamine donor (dihexyloxyTPA) seen in **DP1**, λ_{max} and λ_{onset} values were observed to red-shift by 34 nm and 50 nm respectively. In addition, implementation of the ethylhexyl ester on 3,4-TT seen in **PB1** led to a similar red-shift while also boosting the molar absorptivity of the system to from 22,000 $M^{-1}cm^{-1}$ to 26,000 $M^{-1}cm^{-1}$. Installation of the stronger indoline-based donor present in both **DP2** and **PB2** produced similar optical results to the dihexyloxyTPA donor. A red shift in absorption was viewed in both **DP2** and **PB2** by ~25 nm. Introduction of extended alkyl chains on the 3,4-TT bridge again resulted in higher molar absorptivity values for **PB2** than **DP2** with shorter alkyl chains (30,000 $M^{-1}cm^{-1}$ *vs.* 20,000 $M^{-1}cm^{-1}$). Importantly, addition of hexyloxy chains to the standard TPA donor and the substitution of an indoline-based donor led to a substantial decrease in the optical band gap (E_g^{opt}) when compared to **MCT-1** (~1.85 eV *vs.* 2.00 eV, *Table 1*).

Alterations to the **MCT-1** structure present in all **DP** and **PB** series dyes led to a desirable destabilization in HOMO and LUMO levels, producing dyes with ideal $E_{(S+/S^*)}$ values (-0.77 to -0.79 *vs.* NHE) that do not require lithium doping for electron injection into the TiO_2 semiconductor to occur. The ΔG_{inj} for these improved systems was calculated to be 0.27-0.29 V. $E_{(S+/S)}$ values were measured in order to determine if acceptable electron regeneration could occur between the dye and the I^-/I_3^- redox shuttle. Ground state potentials were measured ranging from 1.08-1.09 V *vs.* NHE. These

potentials are higher than that of **MCT-1**, indicating a lower overpotential for ΔG_{reg} of 0.73-0.74 V. *Figure 10* illustrates a graphical representation of the electrochemical and optical data presented in *Table 1* in order to highlight the decrease in band gap found in both the **DP** and **PB** series dyes and the improvement in oxidation potentials relative to **MCT-1**. These potentials allow for more efficient electron injection into the TiO_2 semiconductor while also enhancing dye regeneration through the I^-/I_3^- redox couple.

Dye	λ_{max} (nm)	ε ($M^{-1}cm^{-1}$)	λ_{onset} (nm)	$E_{(S+/S)}$ (V)	$E_{(S+/S^*)}$ (V)	E_g^{opt} (V)
DP1	558	21800	650	1.09	-0.79	1.88
DP2	591	19600	670	1.08	-0.77	1.85
PB1	560	25700	665	1.09	-0.79	1.88
PB2	584	30000	670	1.08	-0.77	1.85
MCT-1	524	22900	600	1.35	-0.65	2.00

Table 1. Absorbance data and electrochemical data for thienothiophene dyes. Absorbance measurements were taken in DCM solution. The absorption onset (λ_{onset}) was taken at the intercept of the tangent line on the low energy side of the λ_{max} absorption curve and the baseline. $E_{(S+/S)}$ measurements were made in DCM solution using a 0.1 M Bu_4NPF_6 electrolyte and ferrocene as an internal standard. All values are reported *vs.* NHE. $E_{(S+/S^*)}$ were calculated from the equation $E_{(S+/S^*)} = E_{(S+/S)} - E_g^{opt}$. The optical bandgap ($E_g^{opt}$) was calculated from the equation $E_g^{opt} = 1240/\lambda_{onset}$. **MCT-1** measurements are reported in THF solution.[17]

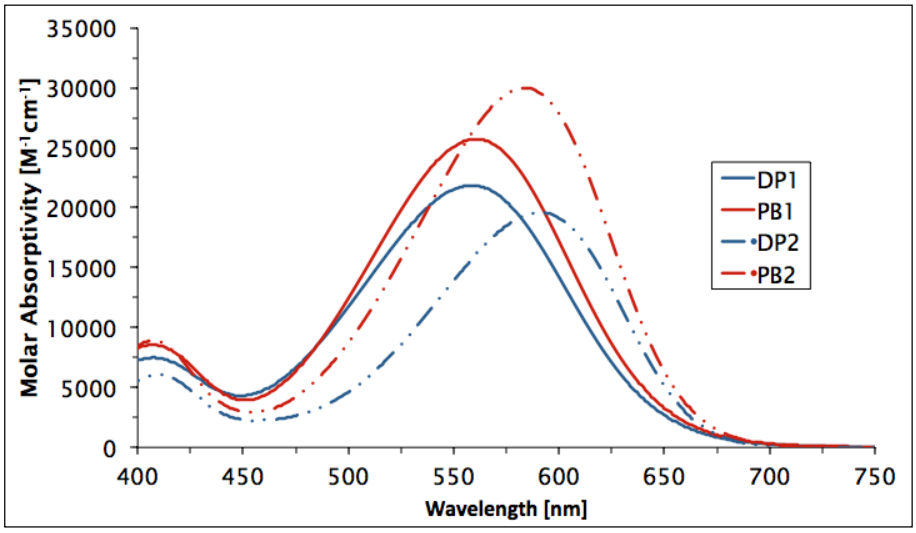

Figure 9. UV-vis absorption spectra of **DP** and **PB** series dyes. All measurements were taken in dichloromethane solution.

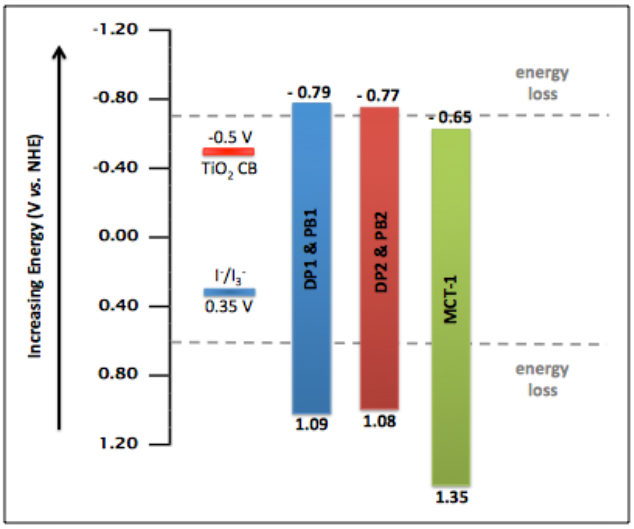

Figure 10. Ground-state and excited-state oxidation potentials of **DP** and **PB** series dyes in comparison to **MCT-1**.

Computational Studies

In order to allow for optimal electron injection into the TiO_2 semiconductor, dyes must possess the correct orbital distribution in addition to favorable oxidation potentials. With regards to the dyes under study, the ideal orbital distribution would indicate high electron density around the acceptor moiety in the LUMO-state. This pattern of orbital distribution is sought after due to the close resemblance in orbital distribution observed between the LUMO-state and the excited-state of these dyes. As shown in the computational studies illustrated in *Figure 11* and *Figure 12*, 3,4-TT dyes carry the bulk of their electron density around the donor subunit in the HOMO-state, with an extensive shift in electron density to the acceptor component upon transition to the LUMO-state. Computational studies conducted on **DP1** and **DP2** indicate an orbital arrangement that is considered ideal for electron injection into the TiO_2 semiconductor.

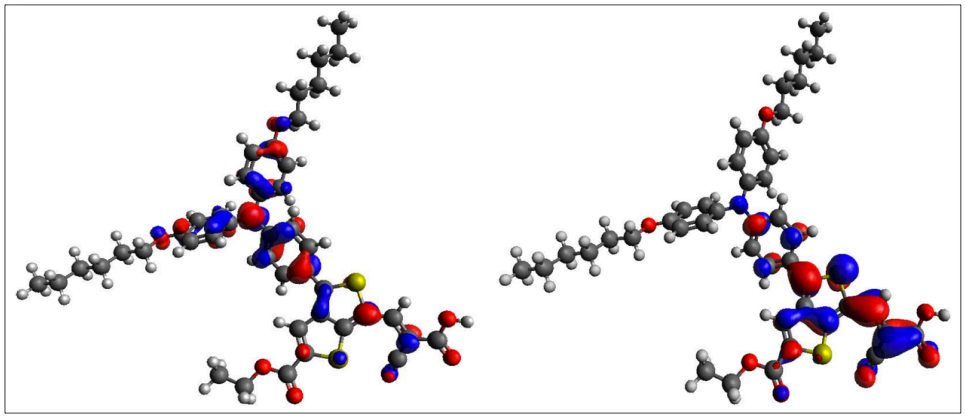

Figure 11. HOMO (left) and LUMO (right) orbitals for **DP1**. (Iso values = 0.035)

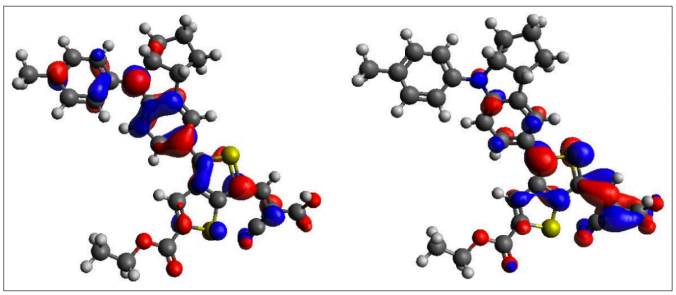

Figure 12. HOMO (left) and LUMO (right) orbitals for **DP2**. (Iso values = 0.035)

Photovoltaic Performance

Having demonstrated favorable electrochemical properties and orbital positions for the use of the thienothiophene series of dyes in DSCs, we have then evaluated their performance in devices with TiO_2 and I^-/I_3 through J-V curve analysis and incident photon-to-current conversion (IPCE) analysis. **DP2** was noted to possess the largest photocurrent density in comparison to all other dyes under study, followed by **PB2**, **PB1**, and **DP1** with a range of 13.7 mA/cm^2 to 10.9 mA/cm^2. This information is illustrated in *Figure 13* and is largely the result of **DP2** exhibiting the greatest absorption range (*Figure 14*) among the **DP** and **PB** series dyes. **DP1** however is shown to produce the lowest J_{SC} value (10.9 mA/cm^2, *Table* 2) due to a narrower absorption range, in addition to a noticeably lower absorbance in the 400-500 nm region. The trend in V_{oc} observed was **PB1** > **DP2** > **DP1** > **PB2** and ranged from 704 mV to 648 mV. As mentioned before, the increase in donor strength present in the **DP** and **PB** series dyes has led to an increase in the excited-state oxidation potential in comparison to **MCT-1**. Due to this increase in the excited-state oxidation potential, lithium doping is no longer required to artificially lower the reduction potential of the TiO_2 semiconductor, thus leading to a significant improvement in V_{OC} and J_{SC} values over that of measurements taken for the

MCT-1 cell. This comprehensive enhancement in electronic parameters produced an increase in overall device performance ranging from 5.61% (**DP1**) to 7.41% (**DP2**).

Electron lifetime measurements were recorded with regards to the **DP** and **PB** series of dyes in order to better understand the observed V_{OC} trends by evaluating the effect of dye structure on electron recombination with the redox shuttle. As stated by Ito, et. al.,[20] addition of long alkyl-substituted groups to the structure of a dye molecule should produce an increase in electron lifetime measurements as the result of preventative recombination of the oxidized redox shuttle with TiO_2 semiconductor electrons. These observations were found to not apply to our 3,4-TT system as seen in *Figure 15*. **DP1** and **DP2** were noted to demonstrate longer electron lifetime measurements than that of the ethylhexyl-substituted **PB2**. This suggests PCE diminishing aggregative effects are not inhibitive for the 3,4-TT π-bridge dyes as the more compact **DP2** gives improved electron lifetimes presumably through a closer packing of the dye on the TiO_2 surface. The expected results were obtained in the case of **PB1**, showing the highest electron lifetime measurements among all of the dyes tested. This is conventional with **PB1** due to the combined sterics present in its ethylhexyl-substituted 3,4-TT π-bridge and its dihexyloxyTPA donor. This slow recombination rate allows **PB1** to generate a higher voltage relative to the other dyes in this series.

Dye	V_{OC} (mV)	J_{SC} (mA/cm^2)	*FF*	η (%)
DP1	680	10.9	0.745	5.61
DP2	697	13.7	0.763	7.41
PB1	704	12.1	0.749	6.50
PB2	648	12.7	0.749	6.24
MCT-1[a]	560	8.80	0.69	3.40

Table 2. Device data measured for **DP** and **PB** series dyes in comparison to **MCT-1**.

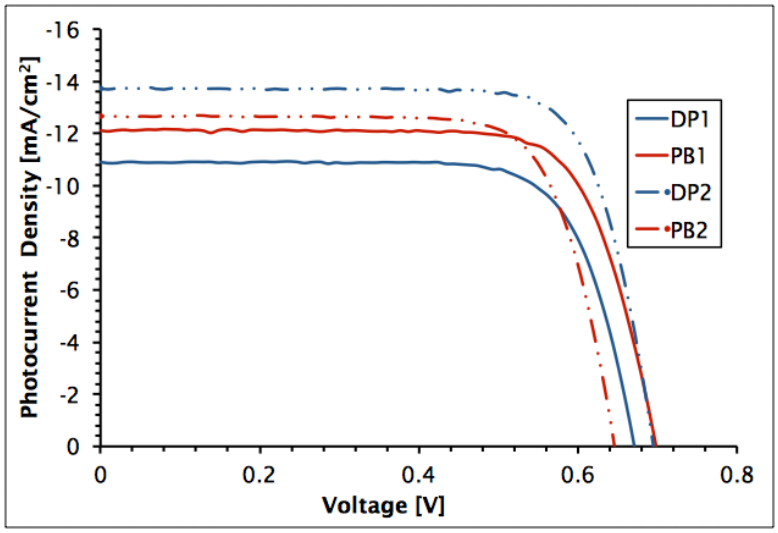

Figure 13. J-V curve of **DP** and **PB** series dyes. (A 450 W xenon lamp at a simulated AM of 1.5 G sun illumination was used as the light source. Measurements were taken using a Z960 electrolyte and I^-/I_3^- redox shuttle. Z960 electrolyte composition: 1.0 M 1,3-dimethylimidazolium iodide, 0.03 M I_2, 0.05 M lithium iodide, 0.01 M guanidinium thiocyanate and 0.5 M *t*-butylpyridine in acetonitrile and valeronitrile solvent mixture (85:15 v/v).)

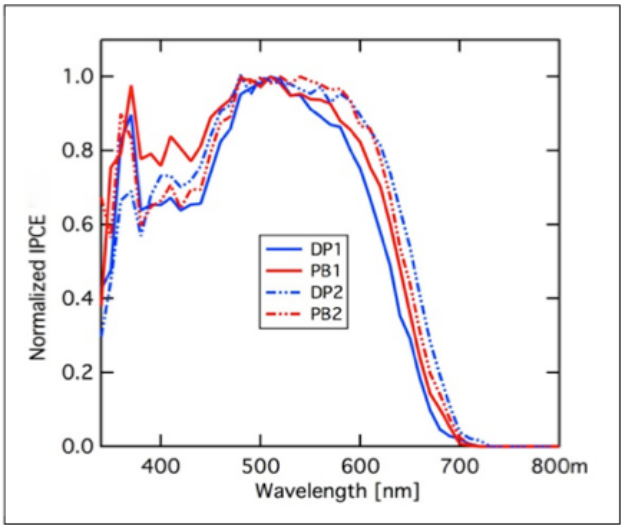

Figure 14. Normalized IPCE absorption spectra for **DP1**, **DP2**, **PB1**, and **PB2** cells.

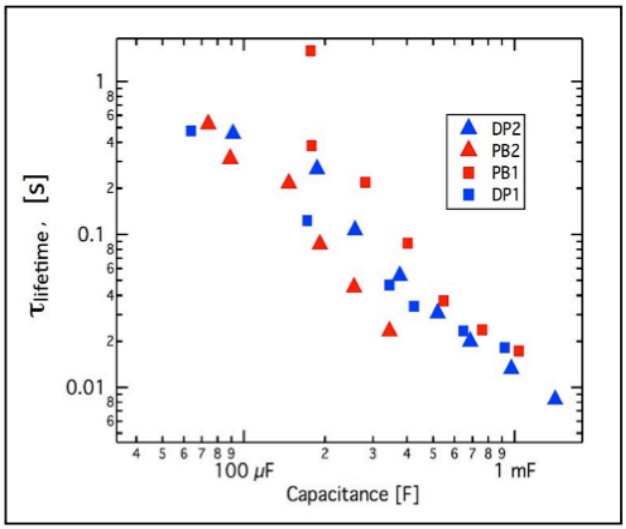

Figure 15. Electron lifetime versus capacitance of **DP1**, **DP2**, **PB1**, and **PB2** cells.

Results and Discussion: Indolizine.

Synthesis: DP3

The synthesis of **DP3** proceeds in 5-synthetic steps according to *Scheme 2*. Commercially available ethyl 3-phenylpropanoate undergoes Friedel-Crafts Acylation to yield chloroacetyl phenyl-ester **1**. Compound **1** is then subjected to base-induced cyclization in the presence of ethyl pyridine to produce the indolizine-ester intermediate **2.** Indolizine-aldehyde **3** is obtained via a Vilsmeier-Haack reaction, installing an aldehyde. Acceptor installation was achieved through condensation of **3** with the tricyanofuran (TCF) moiety, giving rise to **DP3**-ester **4**. Dye **DP3** was completed through hydroxide-ion-promoted ester hydrolysis to give the final dye (**5)** with <10% yield.

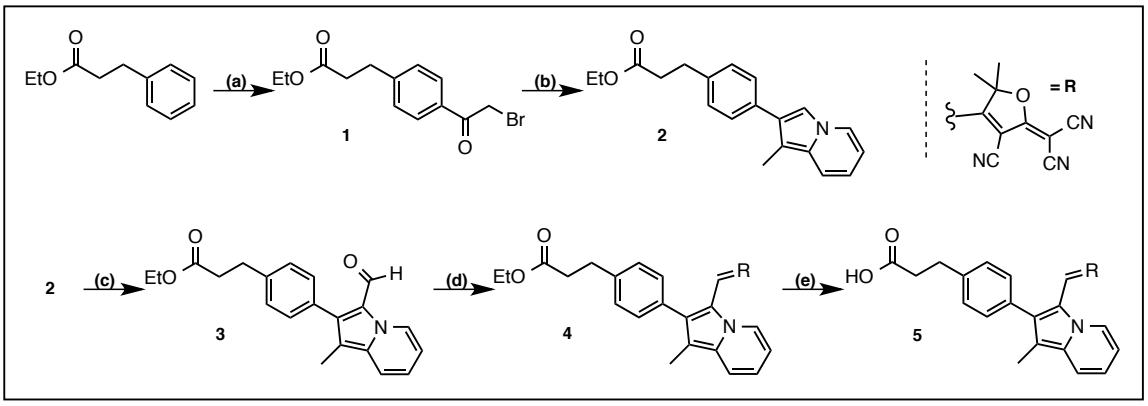

Scheme 2. Synthetic scheme for dye **DP3**. (a) bromoacetyl chloride (1.6 equiv.), 1.8 M DCM, $AlCl_3$ (2.7 equiv.), -5^{0}C to 0^{0}C, 30 min, reflux, 1 hr; carried directly into following reaction. (b) i. ethyl pyridine (1.0 equiv.), 2.0 M acetone, reflux, 24 hr; ii. 24% NaOEt:EtOH (4.0 equiv.), reflux, 24 hr; iii. H_2SO_4 (2.0 mL), EtOH (excess), reflux, 24 hr; 60%. (c) i. 0.4 M DCE, DMF (1.1 equiv.), $POCl_3$ (1.1 equiv.), 0^{0}C to r.t., 1.5 hr; ii. 0.4 M KOH (1.0 M, aq), r.t., 15 min; 60%. (d) TCF (1.1 equiv.), 4-aminophenol (0.4 equiv.), AcOH (0.03 mL), toluene (5.0 mL), reflux, 24 hr; 42%. (e) LiOH (5.0 mL), THF (5.0 mL), r.t., 3.5 hr; , <10%.

Optical and Electrochemical Properties

Implementation of an indolizine-based donor system in place of the tetrahydroquinoline donor seen in **HY103** produced significant changes in optical and electrochemical dye parameters. *Table 3* illustrates the measured absorbance and electrochemical data for **DP3** in comparison to **HY103**. Substitution of the indolizine-based donor in **DP3** was observed to produce a notable red-shift in λ_{max} of 26 nm. Minimal difference in λ_{onset} was recognized. Electrochemical parameters for **DP3** were determined to be less than ideal, demonstrating a ground-state oxidation potential and a

excited-state oxidation potential of 1.22 V and -0.65 V respectively. A graphical representation of the optical and electrochemical data presented in *Table 3* is illustrated in *Figure 16* and *Figure 17,* respectively. The undesirably low $E_{(S+/S^*)}$ value measured for **DP3** raises questions as to if this dye will be effectively able to inject electrons into the TiO_2 semiconductor upon photoexcitation.

Dye	λ_{max} **(nm)**	**ε** **($M^{-1}cm^{-1}$)**	λ_{onset} **(nm)**	$E_{(S+/S)}$ **(V)**	$E_{(S+/S^*)}$ **(V)**	E_g^{opt} **(V)**
DP3	636	203000	664	1.22	-0.65	1.87
HY103	610	66111	660	1.06	-0.87	1.93

Table 3. Absorbance data and electrochemical data for **DP3** compared to **HY103**. Measurements reported for **DP3** were collected using the **DP3-ester** form due to the inherent instability and limited yield of the **DP3** acid. All optical and electrochemical measurements were conducted as stated in the *Table 1* caption. Electrochemical measurements for **HY103** are reported in acetonitrile solution.[19]

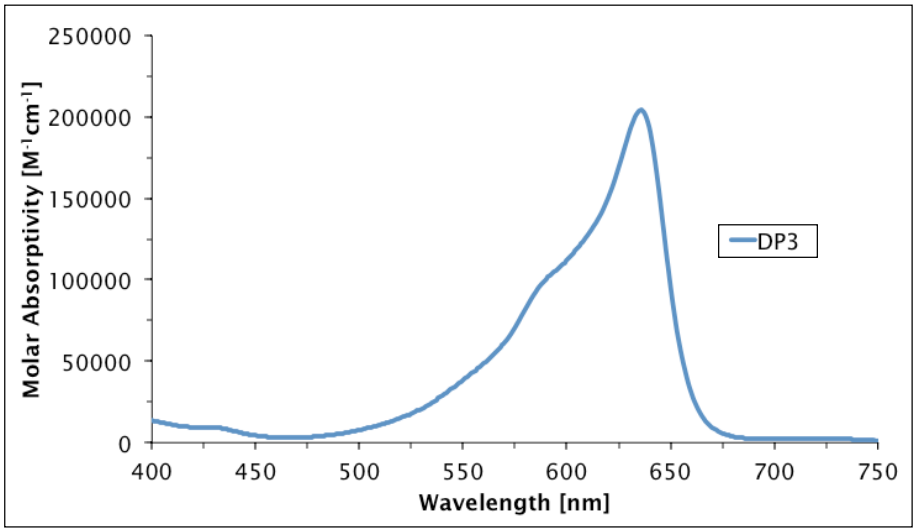

Figure 16. UV-Vis absorption spectrum aproximated for **DP3** obtained via the **DP3-ester** form. All measurements were taken in dichloromethane solution.

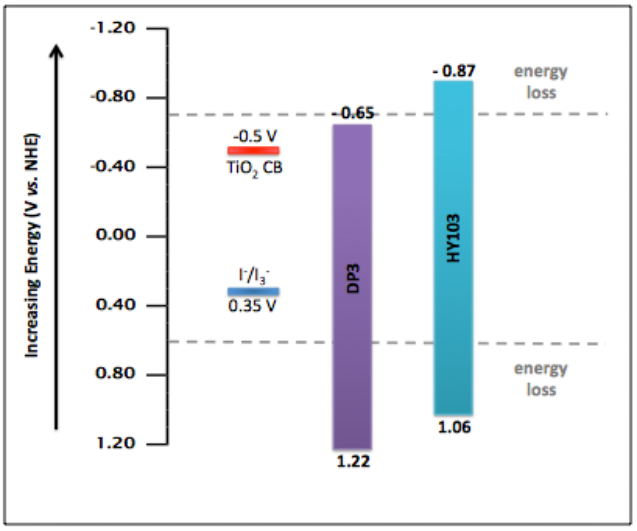

Figure 17. Oxidation and reduction potentials of **DP3** in comparison to **HY103**.

Photovoltaic Performance

Device testing with TiO_2 and I^-/I_3 was conducted using dye **DP3** in order to evaluate cell efficiency. V_{OC} and J_{SC} measurements for **DP3** were determined to be 344 mV and 0.70 mA/cm^2 respectively. The low J_{SC} value is believed to be the result of the relatively narrow absorption range of **DP3** (*Figure 16)* stemming from the planar nature of the **DP3** structure. As expect from the undesirably low $E_{(S+/S^*)}$ value measured for **DP3**, a measured PCE of 0.17% was recorded. It would generally be anticipated that the implementation of a stronger donor moiety would produce increases in $E_{(S+/S^*)}$ values. As follows, this trend would be expected in the case of substituting a stronger indolize-based donor (**DP3**) in place of the tetrahydroquinoline donor seen in **HY103** due to the fact that the same TCF acceptor is utilized in both dye structures. However, this trend is not observed between these dyes. We believe this observation to be the result of the excited-state stabilization of **DP3** leading to a significant reduction in $E_{(S+/S^*)}$ values. Due to this phenomenon seen in **DP3** in conjunction with the strong TCF acceptor, this dye possesses an inherent thermodynamic difficulty with regards to electron injection into the TiO_2 semiconductor.

Dye	V_{OC} (mV)	J_{SC} (mA/cm^2)	*FF*	η (%)
DP3	344	0.70	0.698	0.17
HY103	464	11.76	0.674	3.70

Table 2. Device data measured for dye **DP3** in comparison to **HY103**.

Conclusion.

We have successfully synthesized two series of dyes (**DP** and **PB**) intended for use in dye-sensitized solar cells. The **DP** and **PB** series of dyes were designed to incorporate a pro-aromatic 3,4-TT π-bridge analogous to that of the **MCT-1** dye synthesized by Chen, et. al.[17] Through tuning of the donor subunit we observed a significant reduction in the E_g^{opt}, in comparison to **MCT-1**, leading to an increased range of light absorption. All **DP** and **PB** series dyes demonstrated improved V_{OC} and J_{SC} values, stemming from an excited-state oxidation potential destabilization. This destabilization of the excited-state produced an improved electron injection efficiency to the point at which lithium doping was no longer required to artificially lower the conduction band of the TiO_2 seniconductor, as seen with **MCT-1**. Improvements in these parameters allowed for an increase in cell efficiency ranging from PCEs of 5.61-7.41%. Surprisingly, a shorter electron lifetime measurement was observed in the sterically hindered **PB2** dye in comparison to that of the **DP** series of dyes. With the implementation of minor changes in dye design, we have successfully created more efficient solar cells than previously reported using a 3,4-TT π-bridge moiety.

In addition to the pro-aromatic 3,4-TT dyes, we have synthesized one dye (**DP3**) to incorporate a novel pro-aromatic indolizine-based donor system. This dye was shown to produce a significant red-shift in λ_{max} in comparison to **HY103**, while little change in λ_{onset} was observed. A series of issues with **DP3** were noted with regards to its stability and electrochemical properties. Ground-state and excited-state oxidation potentials measured for **DP3** were not optimal and gave rise to an undesirably low cell efficiency with a PCE value of 0.17%. While overall **DP3** did not provide the desired results, we

believe these issues may be easily adjusted by implementation of a weaker acceptor moiety possessing intermediate electron withdrawing properties in addition to the standard cyanoacrylic acid acceptor. We believe this change would successfully increase the excited-state oxidation potential measured for **DP3** to the point at which efficient electron injection into the TiO_2 semiconductor would be probable. Future work has been gauged toward further experimentation with indolizine-based donors with the intention of correcting issues observed in **DP3**.

References.

[1] U. S. Energy Information Administration, *Annual Energy Review 2010*, October 19, 2011.

[2] BP Global, *Statistical Review of World Energy 2014*, August 26, 2014.

[3] Wheeland M., *The Advantages of Solar Energy vs Other Renewable Energy Sources*, July 22, 2010.

[4] Mishra, A., Fischer, M. K., & Bäuerle, P. (2009). Metal-free organic dyes for dye-sensitized solar cells: From structure: Property relationships to design rules. *Angewandte Chemie International Edition*, *48*(14), 2474-2499.

[5] Ye, M., Wen, X., Wang, M., Iocozzia, J., Zhang, N., Lin, C., & Lin, Z. (2014). Recent advances in dye-sensitized solar cells: from photoanodes, sensitizers and electrolytes to counter electrodes. *Materials Today*.

[6] Hagfeldt, A., Boschloo, G., Sun, L., Kloo, L., & Pettersson, H. (2010). Dye-sensitized solar cells. *Chemical reviews*, *110*(11), 6595-6663.

[7] Thomas, S., Deepak, T. G., Anjusree, G. S., Arun, T. A., Nair, S. V., & Nair, A. S. (2014). A review on counter electrode materials in dye-sensitized solar cells. *Journal of Materials Chemistry A*, *2*(13), 4474-4490.

[8] O'regan, B., & Grfitzeli, M. (1991). A low-cost, high-efficiency solar cell based on dye-sensitized. *nature*, *353*, 24.

[9] Grätzel, M. (2003). Photochemistry reviews. *J Photochem Photobiol C*, *4*, 145-153.

[10] Hardin, B. E., Snaith, H. J., & McGehee, M. D. (2012). The renaissance of dye-sensitized solar cells. *Nature Photonics*, *6*(3), 162-169.

[11] Chen, C. Y., Wang, M., Li, J. Y., Pootrakulchote, N., Alibabaei, L., Ngoc-le, C. H., ... & Grätzel, M. (2009). Highly efficient light-harvesting ruthenium sensitizer for thin-film dye-sensitized solar cells. *ACS nano*, *3*(10), 3103-3109.

[12] Carballo, M. S., Urbani, M., Chandiran, A. K., González-Rodríguez, D., Vázquez, P., Grätzel, M., ... & Torres, T. (2014). Branched and bulky substituted ruthenium sensitizers for dye-sensitized solar cells. *Dalton Transactions*, *43*(40), 15085-15091.

[13] Chiba, Y., Islam, A., Watanabe, Y., Komiya, R., Koide, N., & Han, L. (2006). Dye-sensitized solar cells with conversion efficiency of 11.1%. *Japanese Journal of Applied Physics*, *45*(7L), L638.

[14] Kakiage, K., Aoyama, Y., Yano, T., Otsuka, T., Kyomen, T., Unno, M., & Hanaya, M. (2014). An achievement of over 12 percent efficiency in an organic dye-sensitized solar cell. *Chemical Communications*, *50*(48), 6379-6381.

[15] Mathew, S., Yella, A., Gao, P., Humphry-Baker, R., Curchod, B. F., Ashari-Astani, N., ... & Grätzel, M. (2014). Dye-sensitized solar cells with 13% efficiency achieved through the molecular engineering of porphyrin sensitizers. *Nature chemistry*, *6*(3), 242-247.

[16] Franco, S., Garín, J., Martínez de Baroja, N., Pérez-Tejada, R., Orduna, J., Yu, Y., & Lira-Cantú, M. (2012). New D− π–A-Conjugated Organic Sensitizers Based on 4 H-Pyran-4-ylidene Donors for Highly Efficient Dye-Sensitized Solar Cells. *Organic letters*, *14*(3), 752-755.

[17] Chen, Y. C., Chou, H. H., Tsai, M. C., Chen, S. Y., Lin, J. T., Yao, C. F., & Chen, K. (2012). Thieno [3, 4-b] thiophene-Based Organic Dyes for Dye-Sensitized Solar Cells. *Chemistry-A European Journal*, *18*(17), 5430-5437.

[18] Liu, W. H., Wu, I. C., Lai, C. H., Lai, C. H., Chou, P. T., Li, Y. T., ... & Chi, Y. (2008). Simple organic molecules bearing a 3, 4-ethylenedioxythiophene linker for efficient dye-sensitized solar cells. *Chemical Communications*, (41), 5152-5154.

[19] Hao, Y., Yang, X., Cong, J., Tian, H., Hagfeldt, A., & Sun, L. (2009). Efficient near infrared D–π–A sensitizers with lateral anchoring group for dye-sensitized solar cells. *Chemical Communications*, (27), 4031-4033.

[20] Ito, S., Miura, H., Uchida, S., Takata, M., Sumioka, K., Liska, P., ... & Grätzel, M. (2008). High-conversion-efficiency organic dye-sensitized solar cells with a novel indoline dye. *Chemical Communications*, (41), 5194-5196.

[21] Frisch, M. J., Trucks, G. W., Schlegel, H. B., Scuseria, G. E., Robb, M. A., Cheeseman, J. R., ... & Cross, J. B. (2009). Gaussian 09, revision A. 1. *Gaussian Inc., Wallingford, CT*.

[22] Becke, A. D. (1993). Density-functional thermochemistry. III. The role of exact exchange. *The Journal of Chemical Physics*, *98*(7), 5648-5652.

[23] Miehlich, B., Savin, A., Stoll, H., & Preuss, H. (1989). Results obtained with the correlation energy density functionals of Becke and Lee, Yang and Parr. *Chemical Physics Letters*, *157*(3), 200-206.

[24] Fuller, L. S., Iddon, B., & Smith, K. A. (1997). Thienothiophenes. Part 2. 1 Synthesis, metallation and bromine→ lithium exchange reactions of thieno [3, 2-b] thiophene and its polybromo derivatives. *Journal of the Chemical Society, Perkin Transactions 1*, (22), 3465-3470.

[25] Yu, Q. Y., Liao, J. Y., Zhou, S. M., Shen, Y., Liu, J. M., Kuang, D. B., & Su, C. Y. (2011). Effect of hydrocarbon chain length of disubstituted triphenyl-amine-based organic dyes on dye-sensitized solar cells. *The Journal of Physical Chemistry C*, *115*(44), 22002-22008.

[26] Li, W., Wu, Y., Zhang, Q., Tian, H., & Zhu, W. (2012). DA-π-A featured sensitizers bearing phthalimide and benzotriazole as auxiliary acceptor: effect on absorption and charge recombination dynamics in dye-sensitized solar cells. *ACS applied materials & interfaces*, *4*(3), 1822-1830.

[27] Wang, H., Lu, Z., Lord, S. J., Willets, K. A., Bertke, J. A., Bunge, S. D., ... & Twieg, R. J. (2007). The influence of tetrahydroquinoline rings in dicyanomethylenedihydro-furan (DCDHF) single-molecule fluorophores. *Tetrahedron*, *63*(1), 103-114.

[28] Huckaba, A. J., Giordano, F., McNamara, L. E., Dreux, K. M., Hammer, N. I., Tschumper, G. S., ... & Delcamp, J. H. (2014). Indolizine-Based Donors as Organic Sensitizer Components for Dye-Sensitized Solar Cells. *Advanced Energy Materials*.

Experimental Procedures.

General Information

All commercially obtained reagents were used as received. Thin-layer chromatography (TLC) was conducted with Sigma T-6145 pre-coated Silica gen 60 F_{254} polyester sheets and visualized with UV. Flash column chromatography was performed as described by Still using Sorbent Tech P60, 40-63 μm (230-400 mesh). ^{1}H NMR spectra were recorded on a Bruker Avance-300 (300MHz) spectrometer and are reported in ppm using solvent as an internal standard ($CDCL_3$ at 7.26 ppm). Data reported as: s = singlet, d = doublet, t = triplet, q = quartet, p = pentet, m = multiplet, b = broad, ap = apparent, dd = doublet of doublets; coupling constant(s) in Hz; integration. UV-Vis Spectrum were measured with a Cary 5000 UV-Vis spectrometer. Cyclic voltammetry was measured with a C-H Instruments electrochemical analyzer.

Synthetic Procedures: DP1 and DP2

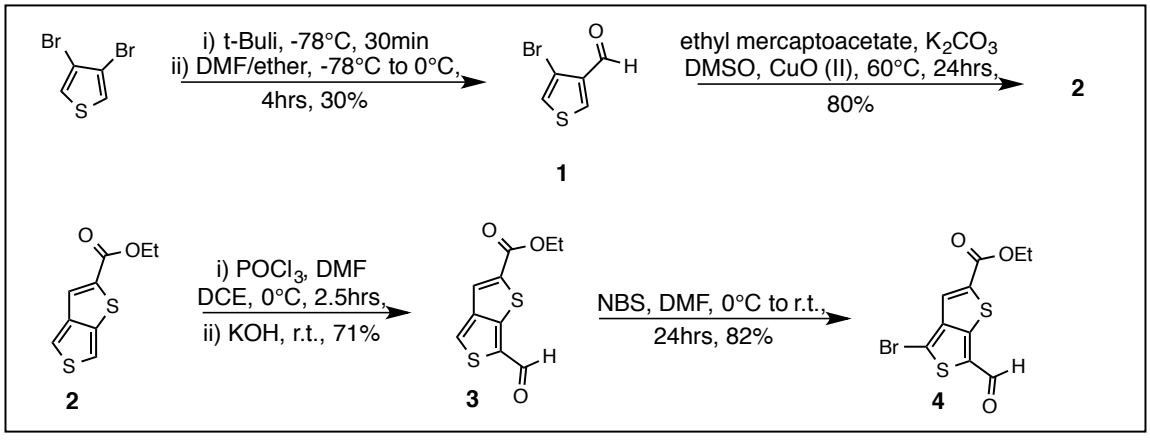

Figure 18. Synthetic route to 3,4-TT acceptor used in dyes **DP1-DP2**.

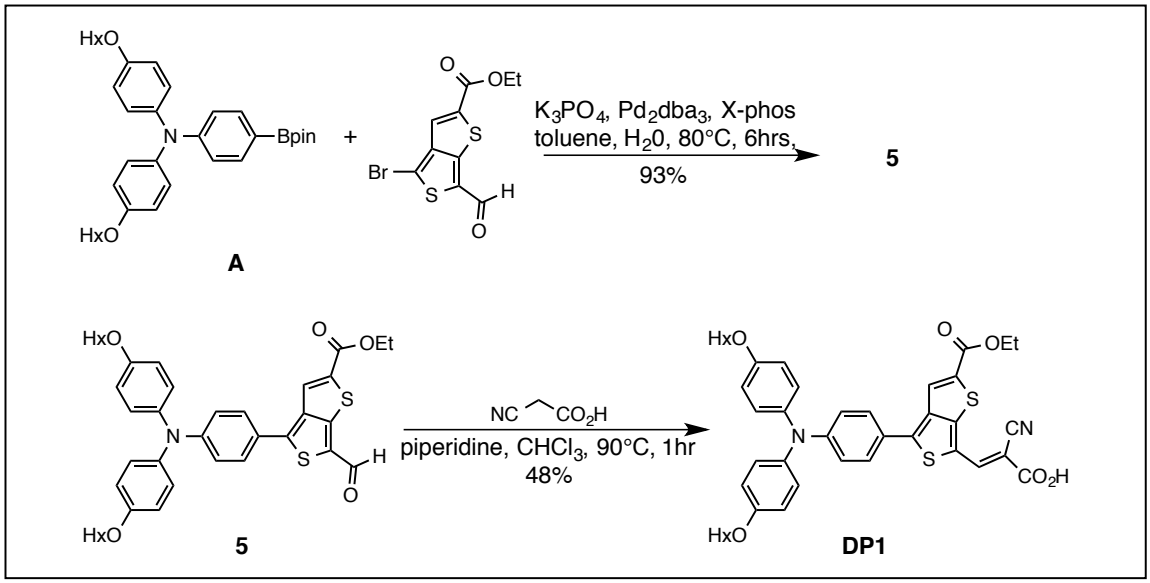

Figure 19. Synthetic route to dye **DP1**. TPA donor **A** was contributed and synthesized by Phillip Brogdon as reported in literature.[25] (**PB1** = substitute ethylhexyl chain for Et)

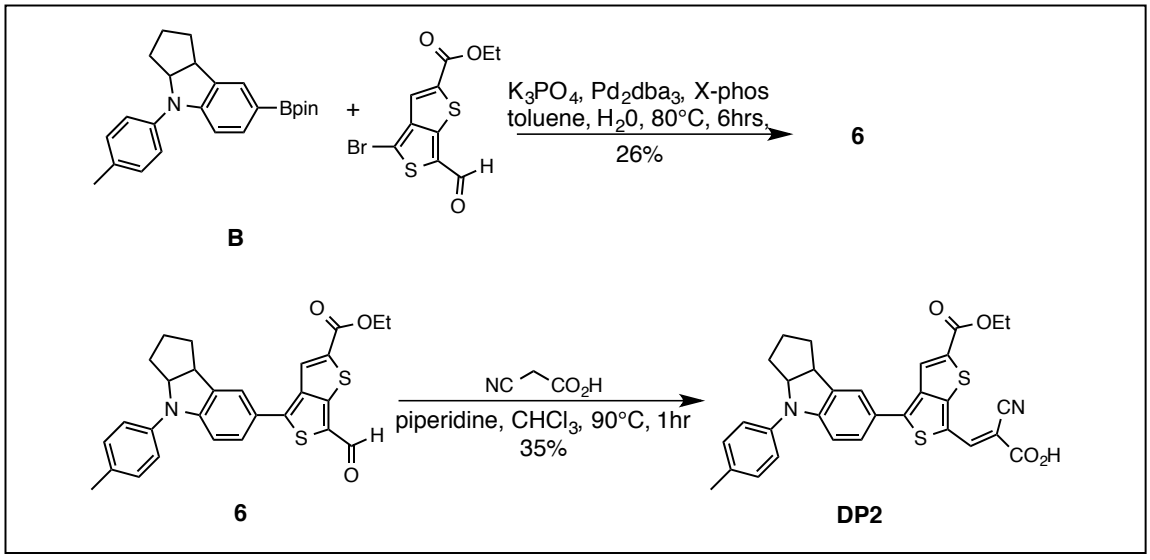

Figure 20. Synthetic route to dye **DP2**. Indoline donor **B** was contributed and synthesized by Phillip Brogdon as reported in literature.[26] (**PB2** = substitute ethylhexyl chain for Et)

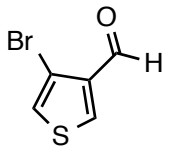

4-bromothiophene-3-carbaldehyde (1):[24] To a flame dried, N_2 filled 200 mL round bottom flask was added dibromothiophene (4.6 mL, 41.3 mmol, 1.0 equiv.) and Et_2O (50.0 mL). The flask was then cooled to -78°C followed by addition of *t*-BuLi (36.4 mL, 62.0 mmol, 1.5 equiv.) dropwise over a 10 minute period. The solution was then stirred for 30 minutes. DMF (3.5 mL, 45.5 mmol, 1.1 equiv.) in Et_2O (25.0 mL) was cooled to -78°C and added slowly to the reaction mixture. The mixture was then allowed to warm to 0°C and stir for 4 hours followed by extraction with excess Et_2O/H_2O and dried over $MgSO_4$. The product was purified through silica gel chromatography with 5% EA:Hx → 10% EA:Hx to give 4-bromothiophene-3-carbaldehyde (2.28 g, 12.0 mmol, 30%). ^{1}H NMR (300MHz, $CDCl_3$) δ 9.95 (s, 1H), 8.16 (d, J = 3.45 Hz, 1H), 7.36 (d, J = 3.45 Hz, 1H).

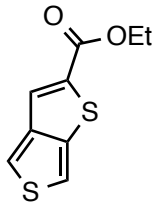

Ethyl thieno[3,4-*b*]thiophene-2-carboxylate (2):[24] To a 100 mL round bottom flask was added 4-bromothiophene-3-carbaldehyde (2.28 g, 12.0 mmol, 1.0 equiv.), K_2CO_3 (3.82 g, 18.0 mmol, 1.5 equiv.), CuO (II) (0.03g, 0.36 mmol, 0.03 equiv.), and DMSO (24.0 mL, 0.5 M). The reaction mixture was heated to 60°C followed by dropwise addition of ethyl mercaptoacetate (1.5 mL, 13.2 mmol, 1.1 equiv.). After stirring for 24 hours the product was purified using a silica gel plug 5% NaOH → 10% NaOH to give ethyl thieno[3,4-*b*]thiophene-2-carboxylate (2.0 g, 9.4 mmol, 79%). ^{1}H NMR (300MHz, $CDCl_3$) δ 7.70 (s, 1H), 7.59 (d, J = 2.58 Hz, 1H), 7.29 (dd, J = 2.7 Hz, 0.9 Hz, 1H), 4.38 (q, J = 7.14 Hz, 2H), 1.40 (t, J = 7.14 Hz, 3H).

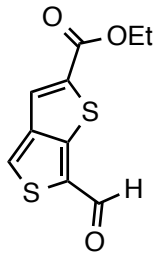

Ethyl 6-formylthieno[3,4-*b*]thiophene-2-carboxylate (3): To a flame dried, N_2 filled 50 mL round bottom flask was added ethyl thieno[3,4-*b*]thiophene-2-carboxylate (0.46 g, 2.2 mmol, 1.0 equiv.), DCE (5.4 mL, 0.4 M), and DMF (0.2 mL, 2.8 mmol, 1.3 equiv.). $POCl_3$ (0.3 mL, 2.8 mmol, 1.3 equiv.) was then added dropwise at 0°C to the reaction mixture. The mixture was allowed to stir at 0°C for a time period of 2.5 hours. The reaction was extracted using excess EA/KOH and dried over $MgSO_4$. The product was purified through silica gel chromatography with 10% EA:Hx → 15% EA:Hx → 20% EA:Hx to give ethyl 6-formylthieno[3,4-*b*]thiophene-2-carboxylate (250.0 mg, 1.5 mmol, 71%). ^{1}H NMR (300MHz, $CDCl_3$) δ 9.92 (s, 1H), 8.04 (s, 1H), 7.77 (s, 1H), 4.38 (q, J = 6.87 Hz, 2H), 1.38 (t, J = 7.14 Hz, 3H).

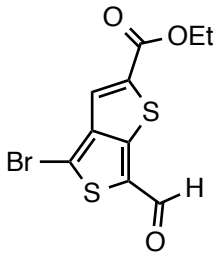

Ethyl 4-bromo-6-formylthieno[3,4-*b*]thiophene-2-carboxylate (4): To a flame dried, N_2 filled 25 mL round bottom flask was added ethyl 6-formylthieno[3,4-*b*] thiophene-2-carboxylate (0.22 g, 0.9 mmol, 1.0 equiv.) and DMF (4.5 mL, 0.2 M). NBS (0.24 g, 1.4 mmol, 1.5 equiv.) was then slowly added to the reaction mixture at 0°C. The mixture was then allowed to warm to room temperature and stir for a time period of 24 hours. The reaction was extracted twice with excess Et_2O/H_2O and dried over $MgSO_4$. The product was purified with a silica gel plug using pure ether to give ethyl 4-bromo-6-formylthieno[3,4-*b*]thiophene-2-carboxylate (234.0 mg, 0.7 mmol, 82%). ^{1}H NMR (300MHz, $CDCl_3$) δ 9.81 (s, 1H), 7.67 (s, 1H), 4.40 (q, J = 7.14 Hz, 2H), 1.40 (t, J = 7.14 Hz, 3H).

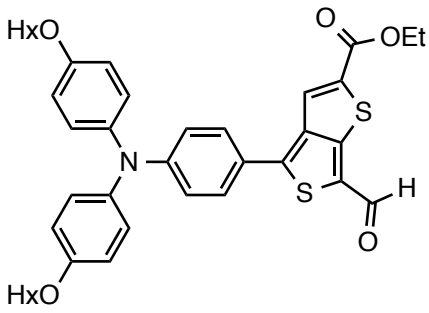

Ethyl 4-(4-(bis(4-(hexyloxy)phenyl)amino)phenyl)-6-formylthieno[3,4-*b*]thiophene-2-carboxylate (5): To a 50 mL round bottom flask was added ethyl 4-bromo-6-formylthieno[3,4-*b*]thiophene-2-carboxylate (50.0 mg, 0.16 mmol, 1.0 equiv.), 4-(hexyloxy)-*N*-(4-(hexyloxy)phenyl)-*N*-(4-(4,4,5,5-tetramethyl-1,3,2-dioxaborolan-2-yl)phenyl)aniline (**A**) (100.0 mg, 0.17 mmol, 1.1 equiv.), K_3PO_4 (100.0 mg, 0.47 mmol, 3.0 equiv.), toluene (3.2 mL, 0.05 M), and H_20 (0.15 mL, 1.1 M). The mixture was allowed to bubble with N_2 for 20 minutes. Pd_2dba_3 (6.0 mg, 0.007 mmol) and X-phos (12.0 mg, 0.025 mmol) were then added simultaneously to the reaction mixture. The temperature was then increased to 80°C and the mixture was allowed to stir for 6 hours. The reaction was then diluted with DCM and dried over $MgSO_4$. The product was purified through silica gel chromatography with 100% DCM → 3% EA:Hx to give ethyl 4-(4-(bis(4-(hexyloxy) phenyl)amino)phenyl)-6-formylthieno[3,4-*b*]thiophene-2-carboxylate (97.0 mg, 0.15 mmol, 93%). ^{1}H NMR (500MHz, $CDCl_3$) δ 9.83 (s, 1H), 7.98 (s, 1H), 7.53 (d, J = 8.60 Hz, 2H), 7.10 (d, J = 8.75 Hz, 4H), 6.93 (d, J = 8.70 Hz, 2H), 6.87 (d, J = 8.80 Hz, 4H), 4.38 (q, J = 7.15 Hz, 2H), 3.94 (t, J = 6.55 Hz, 4H), 1.78 (t, J = 7.05 Hz, 4H), 1.46 (m, 4H), 1.39 (t, J = 7.10 Hz, 3H), 1.34 (m, 8H), 0.90 (b, 6H).

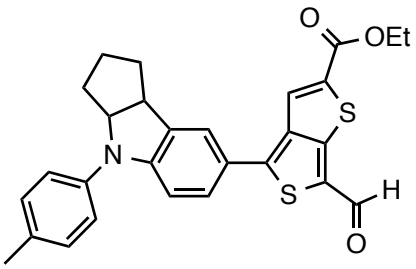

Ethyl 6-formyl-4-(4-(*p*-tolyl)-1,2,3,3a,4,8b-hexahydrocyclopenta[*b*]indol-7-yl)thieno[3,4-*b*]thiophene-2-carboxylate (6): To a 50 mL round bottom flask was added ethyl 4-bromo-6-formylthieno[3,4-*b*]thiophene-2-carboxylate (50.0 mg, 0.16 mmol, 1.0 equiv.), 7-(4,4,5,5-tetramethyl-1,3,2-dioxaborolan-2-yl)-4-(*p*-tolyl)-1,2,3,3a,4,8bhexahydrocyclopenta[*b*]indole (**B**) (64.0 mg, 0.17 mmol, 1.1 equiv.), K_3PO_4 (100.0 mg, 0.47 mmol, 3.0 equiv.), toluene (3.2 mL, 0.05 M), and H_20 (0.15 mL, 1.1 M), and the mixture was allowed to bubble with N_2 for 20 minutes. Pd_2dba_3 (6.0 mg, 0.007 mmol) and X-phos (12.0 mg, 0.025 mmol) were then added simultaneously to the reaction mixture. The temperature was then increased to 80°C and the mixture was allowed to stir for 6 hours. The reaction was then diluted with DCM and dried over $MgSO_4$. The product was purified through silica gel chromatography with 15% EA:Hx → 20% EA:Hx → 25% EA:Hx to give ethyl 6-formyl-4-(4-(*p*-tolyl)-1,2,3,3a,4,8b-hexahydrocyclopenta[*b*]indol-7-yl)thieno[3,4-*b*]thiophene-2-carboxylate (20.0 mg, 0.04 mmol, 26%). ^{1}H NMR (300MHz, $CDCl_3$) δ 9.83 (s, 1H), 8.04 (s, 1H), 7.49 (s, 1H), 7.46 (s, 1H), 7.21 (s, 2H), 6.87 (d, *J* = 8.40 Hz, 1H), 4.91 (t, *J* = 6.39 Hz, 1H), 4.41 (q, *J* = 7.14 Hz, 2H), 3.90 (t, *J* = 8.64 Hz, 1H), 2.37 (s, 3H), 1.93 (m, 2H), 1.74 (m, 2H), 1.59 (m, 2H), 1.41 (t, *J* = 7.11 Hz, 3H).

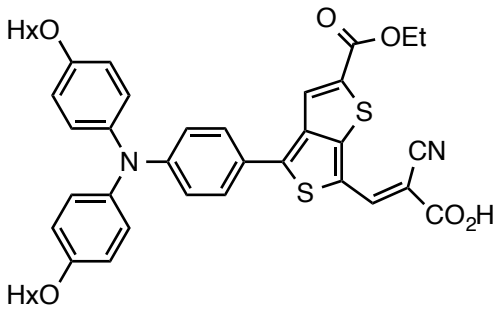

(*E*)-3-(4-(4-(bis(4-(hexyloxy)phenyl)amino)-phenyl)-2-(ethoxycarbonyl)thieno[3,4-*b*]thiophen-6-yl)-2-cyanoacrylic acid (DP1): To a 50 mL round bottom flask was added ethyl 4-(4-(bis(4-(hexyloxy)phenyl)amino)phenyl)-6-formylthieno[3,4-*b*]thiophene-2-carboxylate (36.0 mg, 0.055 mmol, 1.0 equiv.) and $CHCl_3$ (1.0 mL, 0.06 M). The flask was then sealed and allowed to degas with N_2 for 30 minutes. Cyano acetic acid (14.0 mg, 0.166 mmol, 3.0 equiv.) and piperidine (0.04 mL, 0.390 mmol, 7.0 equiv.) were then added and the reaction mixture was heated to 90°C for 1 hour. The reaction mixture was then diluted with DCM and AcOH, extracted twice with DCM/H_2O, and dried over $MgSO_4$. The product mixture was then purified through a silica gel plug with 100% DCM → 3% MeOH:DCM → AcOH. The product solution was then extracted twice with Hx/H_2O and dried over $MgSO_4$ to give (*E*)-3-(4-(4-(bis(4-(hexyloxy)phenyl)amino)phenyl)-2-(ethoxycarbonyl)thieno[3,4-*b*]thiophen-6-yl)-2-cyanoacrylic acid (20.0 mg, 0.026 mmol, 48%). ^{1}H NMR (500MHz, $CDCl_3$) δ 8.36 (s, 1H), 7.98 (s, 1H), 7.60 (m, 2H), 7.11 (d, J = 8.85 Hz, 4H), 6.90 (m, 6H), 4.40 (q, J = 7.2 Hz, 2H), 3.95 (t, J = 6.3 Hz, 4H), 1.78 (t, J = 6.9 Hz, 4H), 1.43 (m, 12H), 0.90 (m 6H), 0.85 (t, J = 8.94, 3H). UV-Vis (CH_2Cl_2): λ_{max} = 559 nm (ε = 22,000 $M^{-1}cm^{-1}$), λ_{onset} = 649 nm. Cyclic Voltammetry (0.1 M Bu_4NPF_6 in CH_2Cl_2, sweep width 1.1-(-2.0), 0.1 V/s scan rate): $E_{(S+/S)}$ = 1.04 V (vs NHE). $E_{(S+/S^*)}$ = -0.87 V [vs NHE, calculated from $E_{(S+/S^*)} = (E_{(S+/S)} - E_g^{opt})$].

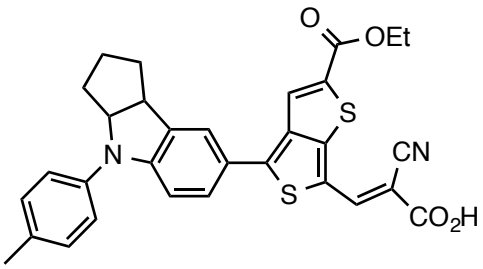

(*E*)-2-cyano-3-(2-(ethoxycarbonyl)-4-(4-(*p*-tolyl)-1,2,3,3a,4,8b-hexahydrocyclopenta[*b*]indol-7-yl)thieno[3,4-*b*]thiophen-6-yl)acrylic acid (DP2): To a 50 mL round bottom flask was added ethyl 6-formyl-4-(4-(*p*-tolyl)-1,2,3,3a,4,8b-hexahydrocyclopenta[*b*]indol-7-yl)-thieno[3,4-*b*]thiophene-2-carboxylate (20.0 mg, 0.041 mmol, 1.0 equiv.) and $CHCl_3$ (1.0 mL, 0.04 M). The flask was then sealed and allowed to degas with N_2 for 30 minutes. Cyano acetic acid (10.0 mg, 0.123 mmol, 3.0 equiv.) and piperidine (0.03 mL, 0.287 mmol, 7.0 equiv.) were then added and the reaction mixture was heated to 90°C for 1 hour. The reaction mixture was then diluted with DCM and AcOH, extracted twice with DCM/H_2O, and dried over $MgSO_4$. The product mixture was then subjected to a silica gel plug using 100% DCM → 3% MeOH:DCM → AcOH. The product solution was then extracted twice with Hx/H_2O, dried over $MgSO_4$, and purified via silica gel chromatography with 2% MeOH:0.5% AcOH:97.5% DCM to give (*E*)-2-cyano-3-(2-(ethoxycarbonyl)-4-(4-(*p*-tolyl)-1,2,3,3a,4,8b-hexahydrocyclopenta[*b*]indol-7-yl)thieno-[3,4-*b*]thiophen-6-yl)acrylic acid (8.0 mg, 0.014 mmol, 35%). ^{1}H NMR (300MHz, $CDCl_3$) δ 8.33 (s, 1H), 8.01 (s, 1H), 7.51 (b, 2H), 7.20 (b, 4H), 6.83 (d, J = 9.24 Hz, 1H), 4.92 (m, 1H), 4.40 (q, J = 6.33 Hz, 2H), 3.87 (m, *1*H), 2.42 (s, 3H), 1.88 (m, 2H), 1.62 (m, 4H), 1.41 (t, J = 7.08 Hz, 3H). UV-Vis (CH_2Cl_2): λ_{max} = 591 nm (ε = 19,000 $M^{-1}cm^{-1}$), λ_{onset} = 664 nm. Cyclic Voltammetry (0.1 M Bu_4NPF_6 in CH_2Cl_2, sweep width 1.1-(-2.0), 0.1 V/s scan rate): $E_{(S+/S)}$ = 1.01 V (vs NHE). $E_{(S+/S^*)}$ = -0.86 V [vs NHE, calculated from $E_{(S+/S^*)} = (E_{(S+/S)} - E_g^{opt})$].

Synthetic Procedures: DP3

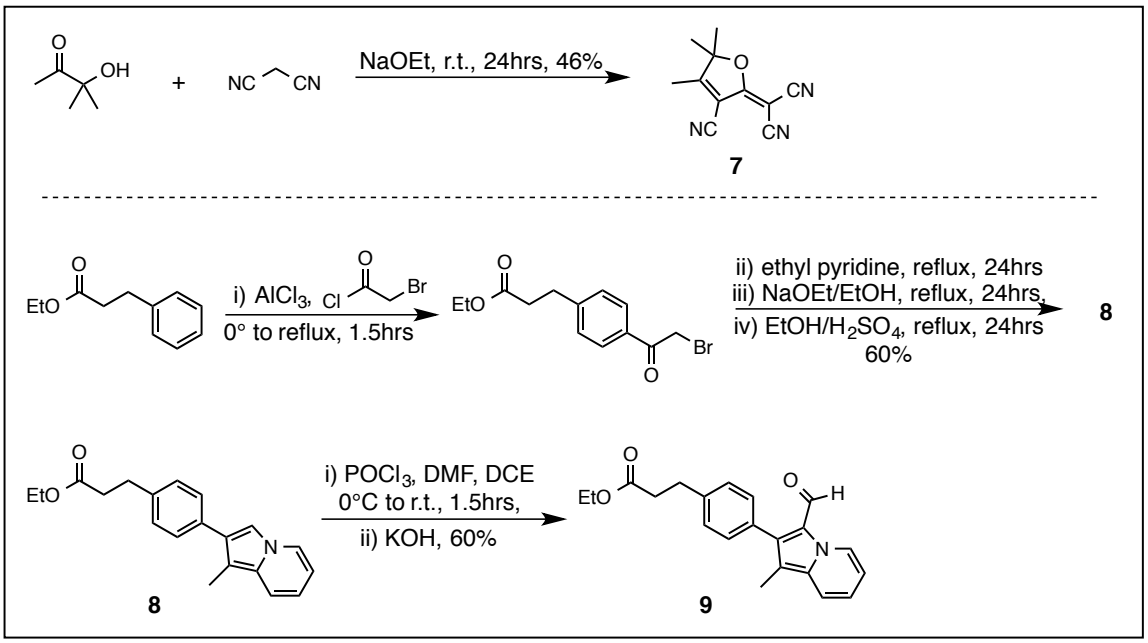

Figure 21. Synthetic route to TCF acceptor (top) and indolizine-based donor (bottom).

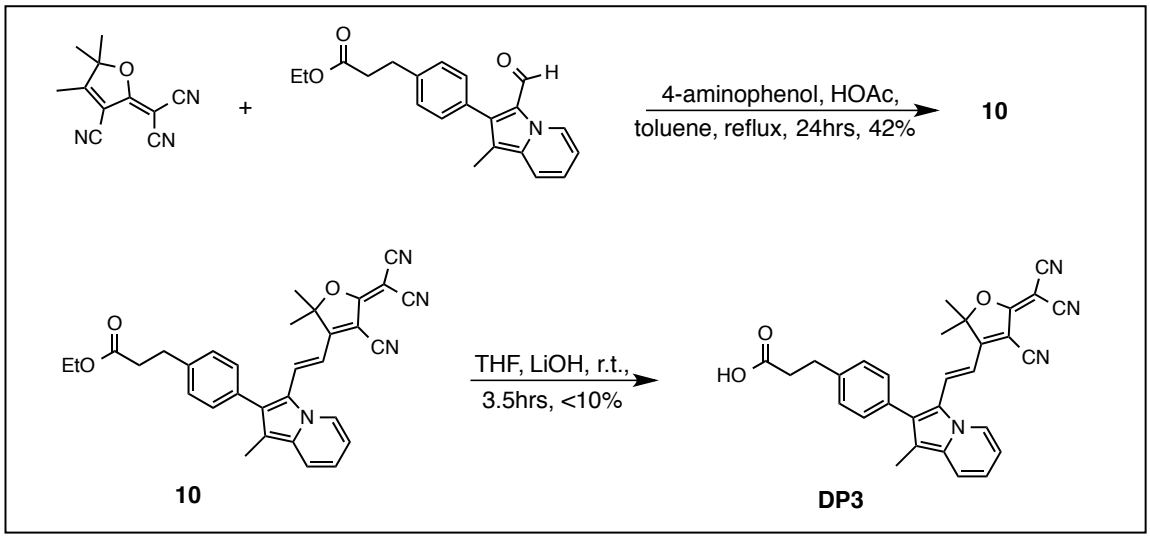

Figure 22. Synthetic route to dye **DP3**.

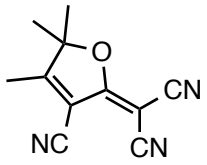

2-(3-cyano-4,5,5-trimethylfuran-2(5*H*)-ylidene)malononitrile (7):[27] To a 100 mL round bottom flask was added 3,3-dimethyl-3-hydroxy propanone (1.68 g, 16.4 mmol, 1.0 equiv.), malononitrile (2.71 g, 41.0 mmol, 2.5 equiv.), and NaOEt (16.5 mL, 1.2 M). The reaction mixture was then allowed to stir at room temperature for 24 hours. The product mixture was then concentrated followed by acidified using 6.0 M aqueous HCl to ~ pH 4-5. The crude product was then filtered off and recrystallized from EtOH to give pure 2-(3-cyano-4,5,5-trimethyl-furan-2(5*H*)-ylidene)malononitrile (1.5 g, 46%). ^{1}H NMR (300MHz, $CDCl_3$) δ 2.35 (s, 3H), 1.62 (s, 6H).

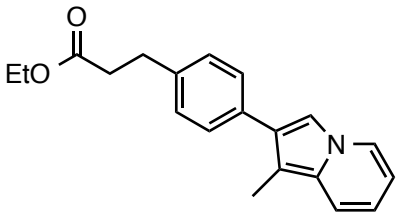

Ethyl 3-(4-(1-methylindolizin-2-yl)phenyl)propanoate (8):[28] To a flame dried, N_2 filled 100 mL round bottom flask was added ethyl 3-phenyl propanoate (3.0 mL, 16.8 mmol, 1.0 equiv) and DCM (9.5 mL, 1.8 M). The flask was then cooled to -5°C and bromoacetyl chloride (2.2 mL, 27.1 mmol, 1.6 equiv.) and $AlCl_3$ (6.1 g, 45.6 mmol, 2.7 equiv.) were added. The reaction mixture was allowed to stir at 0°C for 30 minutes and then subjected to reflux for 1 hour. The mixture was then poured onto ice water, extracted with DCM, dried over $MgSO_4$, and filtered to give the intermediate ethyl 3-(4-(2-bromoacetyl)phenyl)propanoate. To a 150 mL round bottom flask was then added ethyl 3-(4-(2-bromoacetyl)phenyl)propanoate (6.1 g, 23.9 mmol, 1.0 equiv.) and ethyl pyridine (2.7 mL, 23.9 mmol, 1.0 equiv.) in an acetone solution (12.0 mL, 2.0 M). This mixture was allowed to reflux for 24 hours. Acetone was then removed from the reaction mixture, followed by the addition of 21% NaOEt:EtOH (35.0 mL, 95.6 mmol, 4.0

equiv.). This mixture was then again allowed to reflux for 24 hours. The product obtained at this point was noted to be completely water soluble and it was hypothesized that the ester chain α position had been deprotonated. The product mixture was then transferred to a 1 L flask using H_2O (500.0 mL) and the pH of the solution was adjusted to pH 5-6 using AcOH. The product mixture was then extracted using DCM/H_2O. NMR analysis showed presence of acid product due to ester chain hydrolysis. The acid product, EtOH (300.0 mL), and H_2SO_4 (2.0 mL) were then added to a 1 L round bottom flask and allowed to reflux for 24 hours. The product mixture was then extracted with DCM/H_2O and dried over $MgSO_4$ to give pure ethyl 3-(4-(1-methylindolizin-2-yl)phenyl)propanoate (3.1g, 10.1 mmol, 60%). ^{1}H NMR (300MHz, $CDCl_3$) δ 7.84 (d, J = 6.93 Hz, 1H), 7.44 (d, J = 8.01 Hz, 2H), 7.36 (s, 1H), 7.32 (b, 1H), 7.29 (b, 2H), 6.60 (t, J = 7.02 Hz, 1H), 6.40 (t, J = 6.21 Hz, 1H), 4.15 (q, J = 7.11 Hz, 2H), 2.99 (t, J = 7.41 Hz, 2H), 2.66 (t, J = 8.16 Hz, 2H), 2.41 (s, 3H), 1.21 (t, J = 5.88 Hz, 3H).

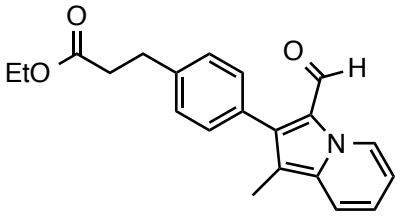

Ethyl 3-(4-(3-formyl-1-methylindolizin-2-yl)phenyl)-propanoate (9): To a 50 mL round bottom flask was added ethyl 3-(4-(1-methylindolizin-2-yl)phenyl)prop-anoate (1.0 g, 3.25 mmol, 1.0 equiv.). The flask was then subjected to an N_2/vacuum cycle followed by the addition of DCE (8.1 mL, 0.4 M) and anhydrous DMF (0.28 mL, 3.58 mmol, 1.1 equiv.). The flask was then cooled to 0°C and $POCl_3$ (0.33 mL, 3.58 mmol, 1.1 equiv.) was added dropwise by syringe. The reaction was then allowed to warm to room temperature and stir for 1.5 hours. The product mixture was extracted with excess DCM/KOH. Purification was obtained via silica gel chromatography with 100%

DCM → 20% EA:DCM to give ethyl 3-(4-(3-formyl-1-methylindolizin-2-yl)phenyl)-propanoate (640.0 mg, 1.95 mmol, 60%). ^{1}H NMR (300MHz, $CDCl_3$) δ 9.81 (d, *J* = 6.96 Hz, 1H), 9.51 (s, 1H), 7.52 (d, *J* = 8.91 Hz, 2H), 7.30 (d, *J* = 8.16 Hz, 2H), 7.21 (t, 1H), 6.91 (t, *J* = 7.08 Hz, 1H), 4.13 (q, *J* = 7.14 Hz, 2H), 3.03 (t, *J* = 7.5 Hz, 2H), 2.68 (t, *J* = 8.19 Hz, 2H), 2.26 (s, 3H), 1.25 (t, *J* = 7.11 Hz, 3H).

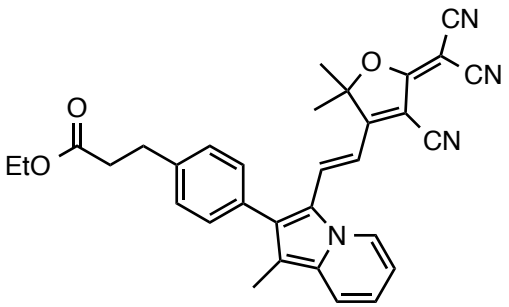

Ethyl (*E*)-3-(4-(3-(2-(4-cyano-5-(dicyano-methylene)-2,2-dimethyl-2,5-dihydrofuran-3-yl)vinyl)-1-methylindolizin-2-yl)phenyl)prop-anoate (10): To a flame dried, N_2 filled round bottom flask was added ethyl 3-(4-(3-formyl-1-methylindolizin-2-yl)phenyl) propanoate (77.0 mg, 0.23 mmol, 1.0 equiv), 2-(3-cyano-4,5,5-trimethylfuran-2(5*H*)-ylidene)malononitrile (50.0 mg, 0.25 mmol, 1.1 equiv.), 4-aminophenol (10.9 mg, 0.10 mmol, 0.4 equiv.), AcOH (0.03 mL), and toluene (5.0 mL). The reaction mixture was then heated to 120°C and allowed to reflux under dean-stark setup for 24 hours. The product mixture was extracted using excess DCM/H_2O, and then dried over Na_2SO_4. Purification was achieved using silica gel chromatography with 100% DCM → 3% EA:DCM → 5% EA:DCM → 10% EA:DCM to give ethyl (*E*)-3-(4-(3-(2-(4-cyano-5-(dicyanomethylene)-2,2-dimethyl-2,5-dihydrofuran-3-yl)vinyl)-1-methylindolizin-2-yl)phenyl)propanoate (50.0 mg, 0.01 mmol, 42% yield). ^{1}H NMR (300MHz, $CDCl_3$) δ 8.42 (d, *J* = 7.29 Hz, 1H), 7.55 (d, *J* = 8.19 Hz, 1H), 7.39 (s, 2H), 7.36 (s, 2H), 7.09 (t, *J* = 5.91 Hz, 2H), 4.13 (q, *J* = 7.05 Hz, 2H), 3.05 (t, *J* = 7.98 Hz, 2H), 2.68 (t, *J* = 7.71 Hz, 2H), 2.19 (s, 3H), 2.01 (s, 6H), 0.84 (t, *J* = 8.13 Hz, 3H). UV-

Vis (CH_2Cl_2): λ_{max} = 638 nm (ε = 57,000 $M^{-1}cm^{-1}$), λ_{onset} = 664 nm. Cyclic Voltammetry (0.1 M Bu_4NPF_6 in CH_2Cl_2, sweep width 1.1-(-2.0), 0.1 V/s scan rate): $E_{(S+/S)}$ = 1.22 V (vs NHE). $E_{(S+/S^*)}$ = -0.65 V [vs NHE, calculated from $E_{(S+/S^*)} = (E_{(S+/S)} - E_g^{opt})$].

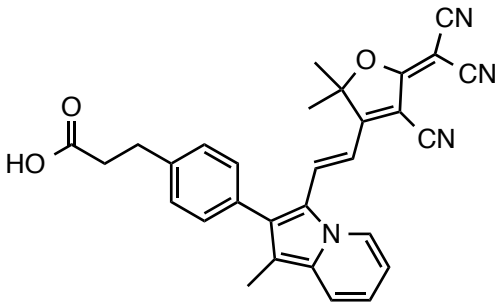

(*E*)-3-(4-(3-(2-(4-cyano-5-(dicyanomethylene) -2,2-dimethyl-2,5-dihydrofuran-3-yl) vinyl)1-methylindolizin-2-yl)phenyl)propanoic acid (DP3): To a 50 mL round bottom flask was added ethyl (*E*)-3-(4-(3-(2-(4-cyano-5-(dicyano-methylene)-2,2-dimethyl-2,5-dihydrofuran-3-yl)vinyl)-1-methylindolizin-2-yl)phenyl)-propanoate (38.0 mg, 0.74 mmol, 1.0 equiv.), LiOH (5.0 ml), and THF (5.0 mL). The reaction mixture was allowed to stir at room temperature for 3.5 hours. Next, the reaction mixture was diluted with 5% AcOH:DCM (100.0 mL), and washed 3 times with excess H_2O. Product purification was attempted via an alumina plug with 100% DCM → 5% MeOH:DCM → 10% MeOH:DCM → 20% MeOH:DCM → 50% MeOH:DCM → 100% MeOH → 3% AcOH:MeOH. The product mixture was then extracted with excess DCM/H_2O, and dried over Na_2SO_4. NMR analysis showed product decomposition along with the presence of the desired product, (*E*)-3-(4-(3-(2-(4-cyano-5-(dicyanomethylene)-2,2-dimethyl-2,5-dihydrofuran-3-yl)vinyl)-1-methylindolizin-2-yl)phenyl)propanoic acid (<10%). UV-Vis spectrum and cyclic voltammetry measurements for DP3 were approximated using compound **10**, ethyl (*E*)-3-(4-(3-(2-(4-cyano-5-(dicyanomethylene)-2,2-dimethyl-2,5-dihydrofuran-3-yl)vinyl)-1-methylindolizin-2-yl)phenyl)propanoate. ^{1}H NMR (300MHz, $CDCl_3$) δ 8.43 (d, *J* = 6.33 Hz, 1H), 7.55 (m, 1H), 7.38 (m, 4H), 7.19

(m, 1H), 7.11 (m, 1H), 3.06 (t, J = 6.9 Hz, 2H), 2.74 (t, J = 7.14 Hz, 2H), 2.26 (s, 3H), 2.19 (s, 6H).

Computational Details

All computations were performed with the Gaussian09[21] software package. The geometry optimization for dyes **DP1** and **DP2** were as follows: first the structures were optimized by MM2 in the ChemBio3D (version: 13.0.2.3021) software package and dihedral angles for all relevant groups set to values in-between the global minimum and the next local maximum on the conformational energy diagram as calculated by ChemBio3D (version: 13.0.2.3021) in the dihedral driver toolset. After MM2 optimization, the molecular structures were further optimized by DFT methods: first B3LYP/3-21G[22,23] and then B3LYP/6-311G(d,p)[22,23]. Lastly, time-dependent density functional theory (TD-DFT) computations were carried out to compute the vertical transition energies and oscillator strengths for the 10 lowest excited states. Symmetry was explicitly turned off for these computations even though all of the optimized structures belonged to the C_1 point group. A representative TD-DFT input file is included for both **DP1** and **DP2**.

Photovoltaic Characterization

A 450W xenon lamp (Oriel, USA) was used as a light source to study the current-voltage characteristics of the DSSC. The spectral output of the lamp was filtered using a Schott K113 Tempax sunlight filter (Präzisions Glas & Optik GmbH, Germany) to reduce the mismatch between the simulated and actual solar spectrum to less than 2 %.

The Keithley model 2400 digital source meter (Keithley, USA) was used for data acquisition. The photo-active area of 0.16 cm^2 was defined by a black mask of 6x6 mm^2. Incident photon-to-current conversion efficiency measurements were carried from the mono chromated visible photons, from Gemini-180 double monochromator Jobin Yvon Ltd. (UK), powered by a 300 W xenon light source (ILC Technology, USA) superimposed on a 10mW/cm^2 LED light. The monochromatic incident light was passed through a chopper running at 2 Hz frequency and the on / off ratio was measured by an operational amplifier.

Device Fabrication

The photoanode consists of thin TiO_2 electrodes comprising a 9.5 mm mesoporous TiO_2 layer (particle size, 20 nm) and a 5.0 mm TiO_2 scattering layer (particle size, 400 nm). The working electrode was prepared by immersing the 14.5 mm (9.5 mm thick transparent layer + 5.0 mm thick scattering) TiO_2 film into the dye solution for 18 h. A thermally platinized FTO glass counter electrode and the working electrode were then sealed with a 25 mm thick hot-melt film (Surlyn, Dupont) by heating the system at 100°C. Devices were completed by filling the electrolyte by pre-drilled holes in the counter electrodes and finally the holes were sealed with a Surlyn sheet and a thin glass cover by heating. A black mask (6x6 mm^2) was used in the subsequent photovoltaic studies.

^{1}H NMR Data.

^{1}H NMR: 4-bromothiophene-3-carbaldehyde (1)

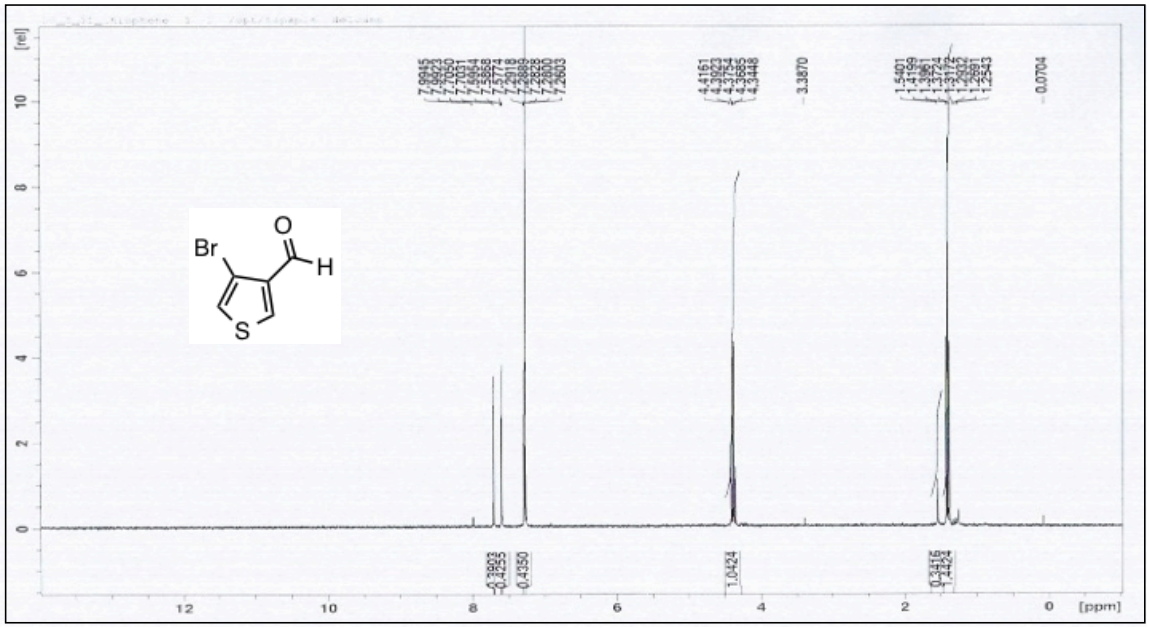

^{1}H NMR: Ethyl thieno[3,4-*b*]thiophene-2-carboxylate (2)

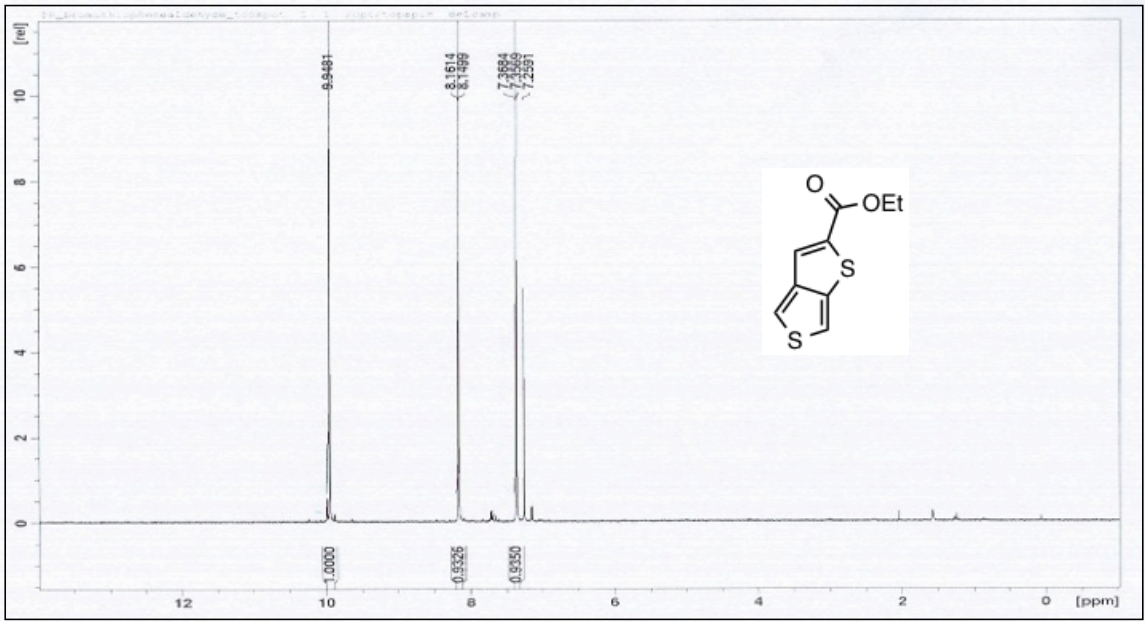

^{1}H NMR: Ethyl 6-formylthieno[3,4-*b*]thiophene-2-carboxylate (3)

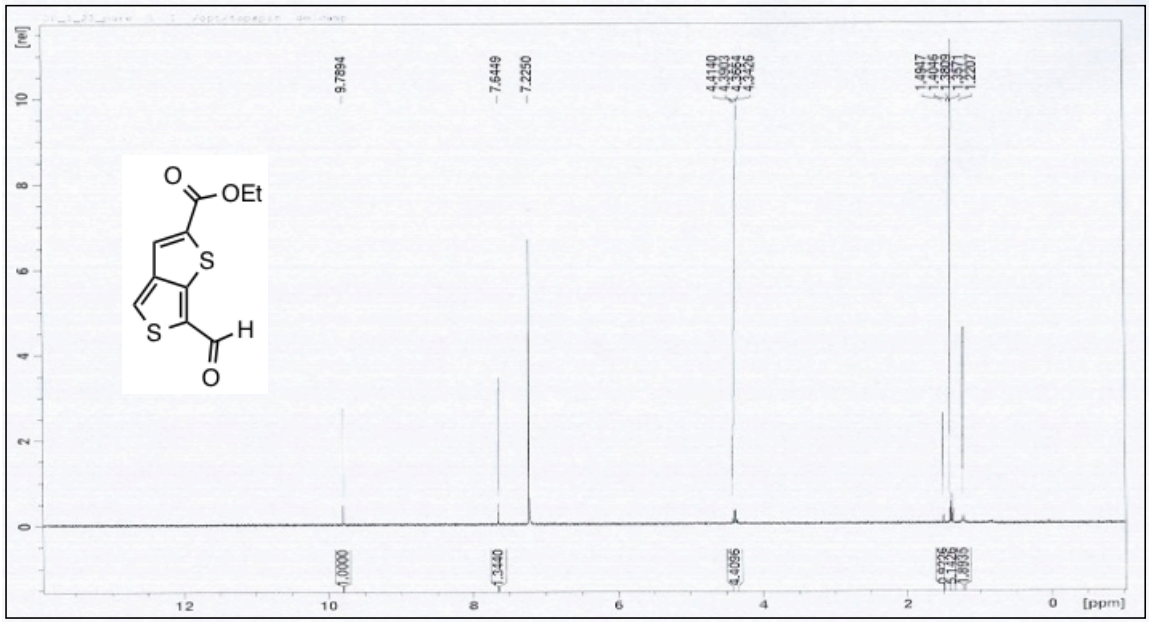

^{1}H NMR: Ethyl 4-bromo-6-formylthieno[3,4-*b*]thiophene-2-carboxylate (4)

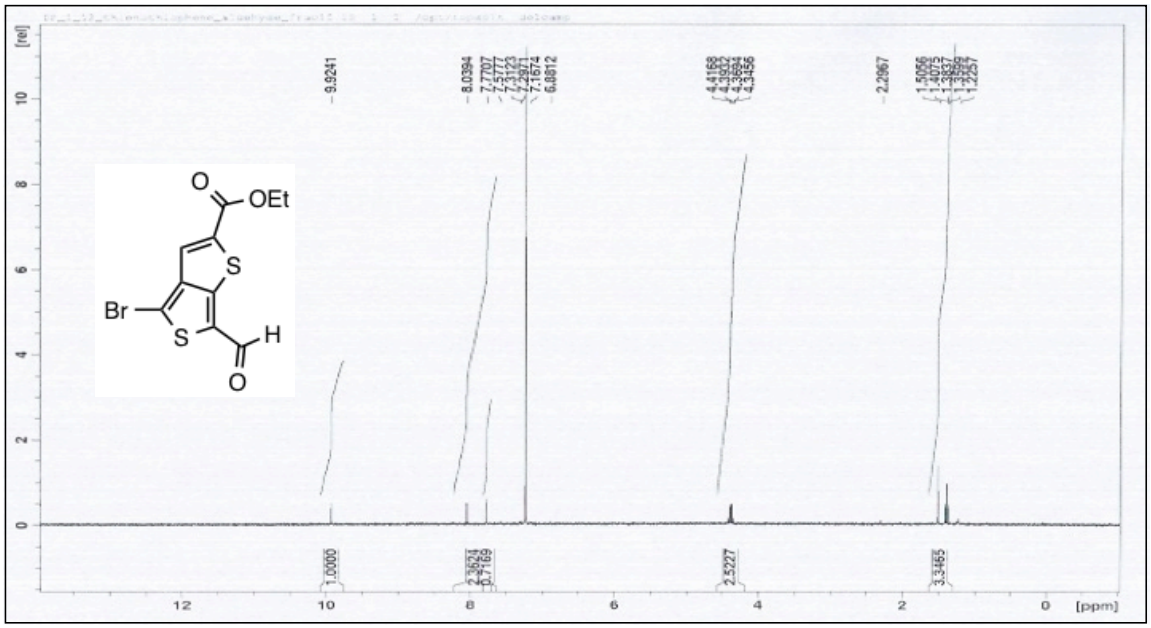

^{1}H NMR: Ethyl 4-(4-(bis(4-(hexyloxy)phenyl)amino)phenyl)-6-formylthieno[3,4-*b*] thiophene-2-carboxylate (5)

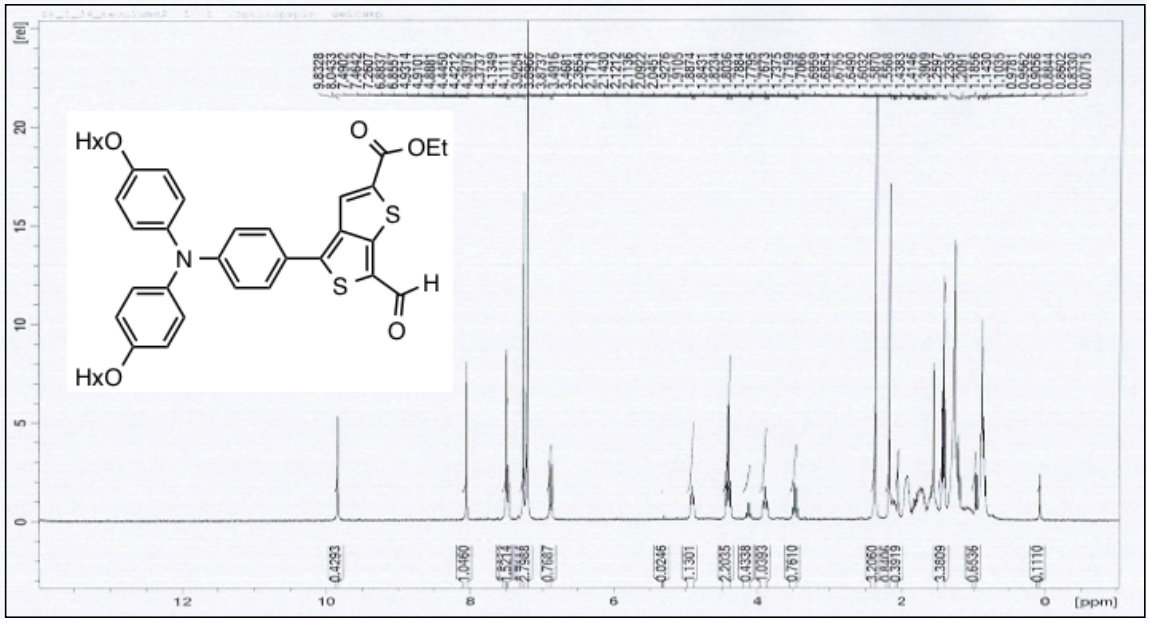

^{1}H NMR: Ethyl 6-formyl-4-(4-(*p*-tolyl)-1,2,3,3a,4,8b-hexahydrocyclopenta[*b*]indol-7-yl)thieno[3,4-*b*]thiophene-2-carboxylate (6)

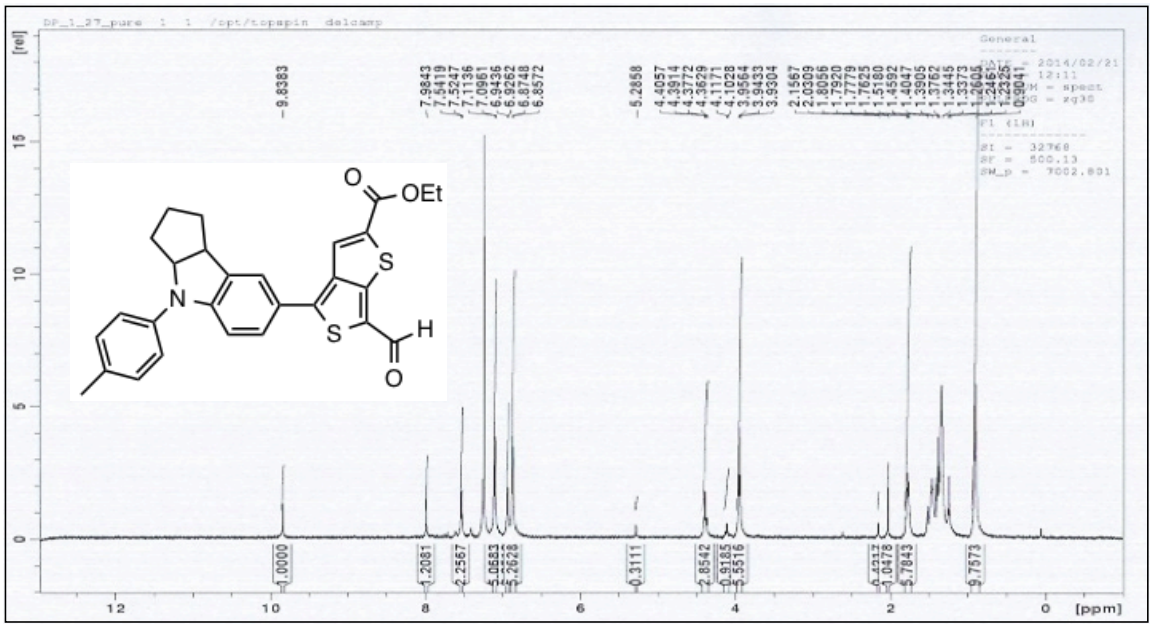

^{1}H NMR: (*E*)-3-(4-(4-(bis(4-(hexyloxy)phenyl)amino)phenyl)-2-(ethoxycarbonyl) thieno[3,4-*b*]thiophen-6-yl)-2-cyanoacrylic acid (DP1)

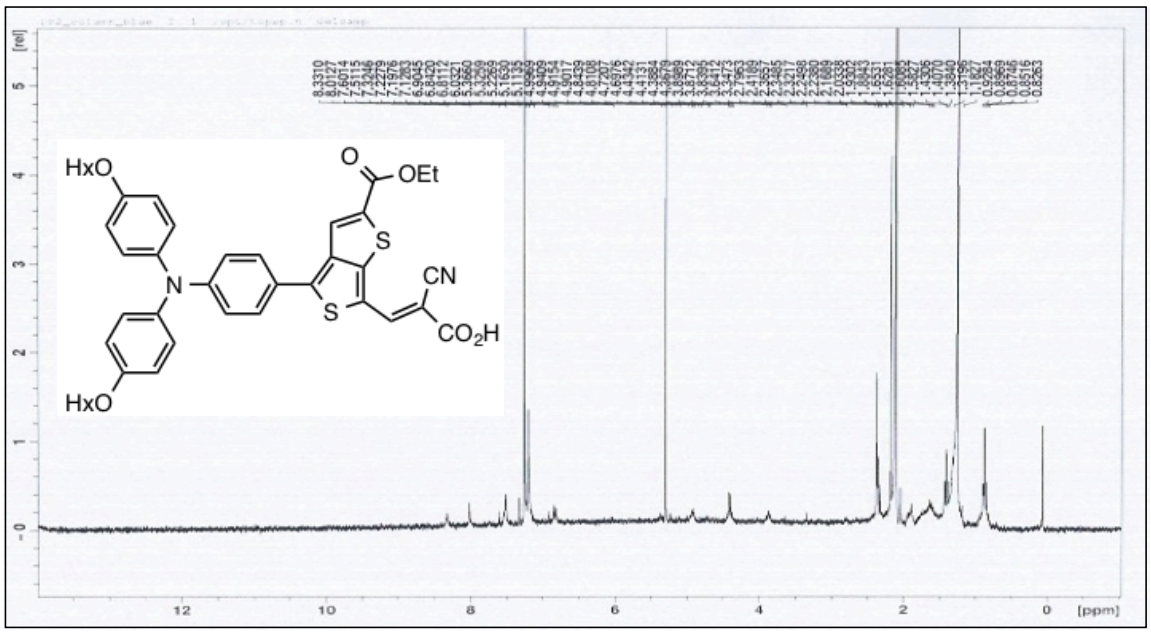

^{1}H NMR: (*E*)-2-cyano-3-(2-(ethoxycarbonyl)-4-(4-(*p*-tolyl)-1,2,3,3a,4,8b-hexa hydrocyclopenta[*b*]indol-7-yl)thieno[3,4-*b*]thiophen-6-yl)acrylic acid (DP2)

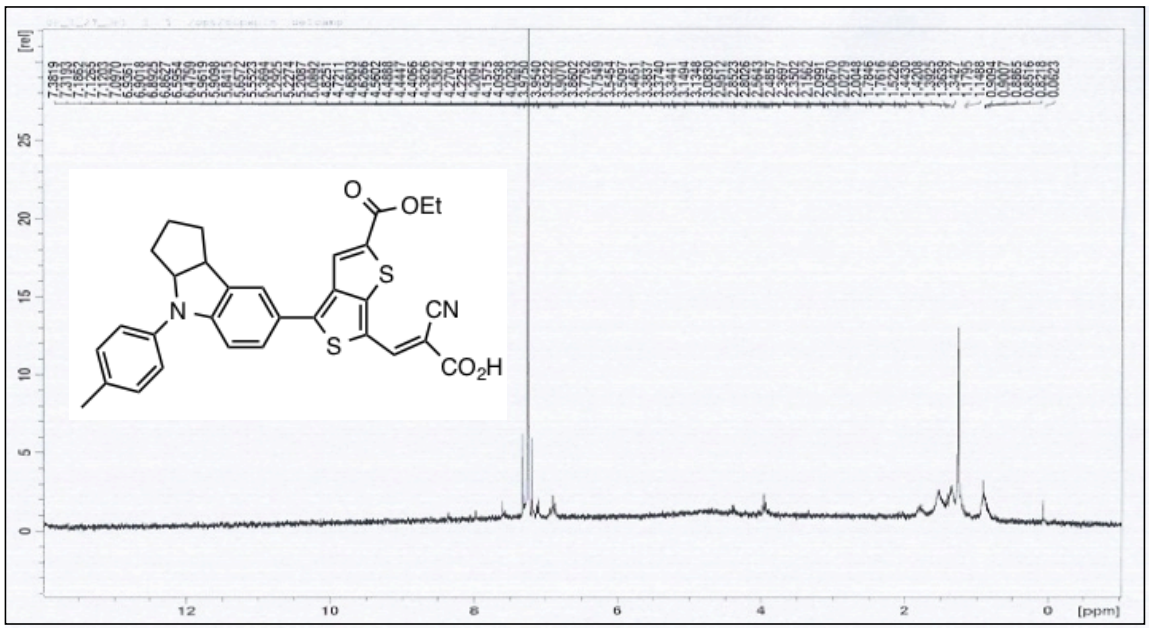

^{1}H NMR: 2-(3-cyano-4,5,5-trimethylfuran-2(5*H*)-ylidene)malononitrile (7)

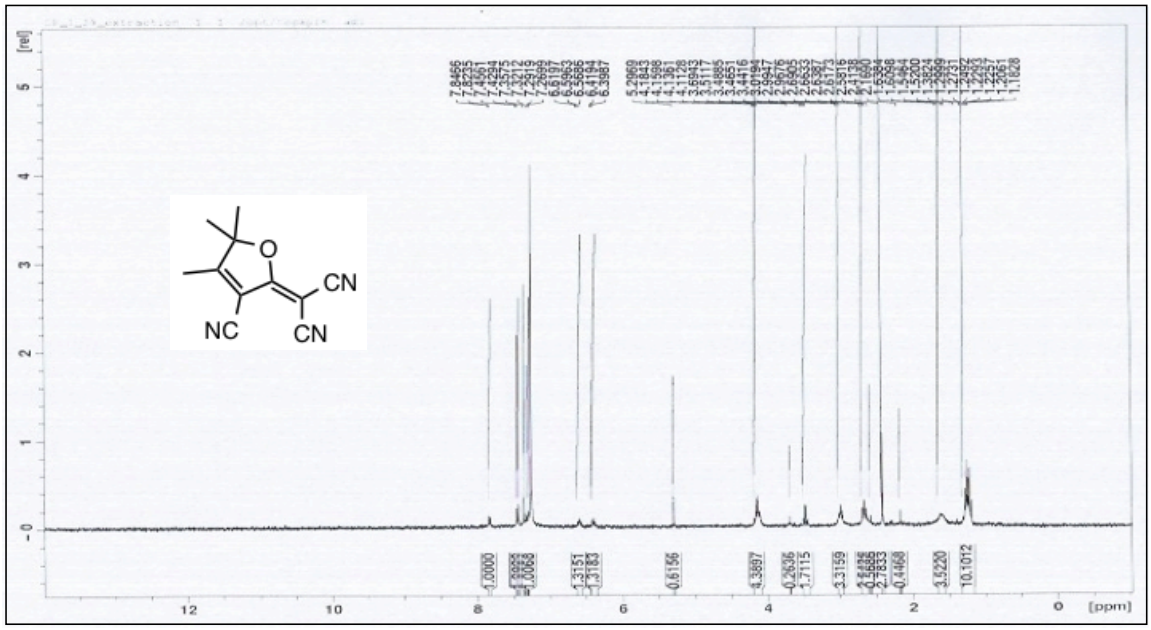

^{1}H NMR: Ethyl 3-(4-(1-methylindolizin-2-yl)phenyl)propanoate (8)

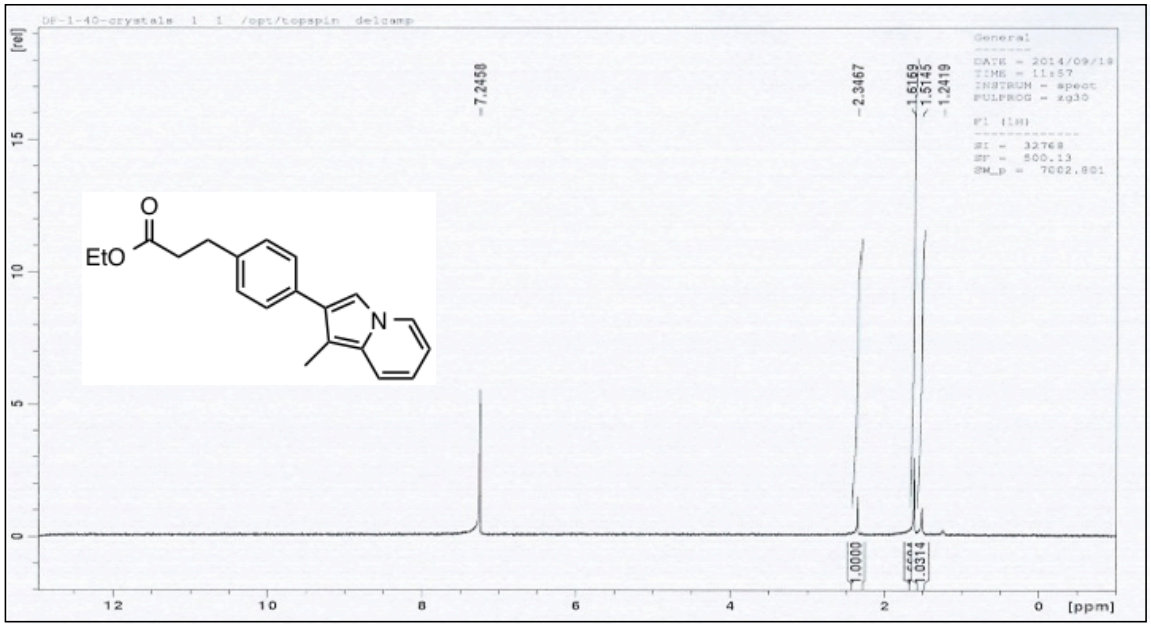

^{1}H NMR: Ethyl 3-(4-(3-formyl-1-methylindolizin-2-yl)phenyl)propanoate (9)

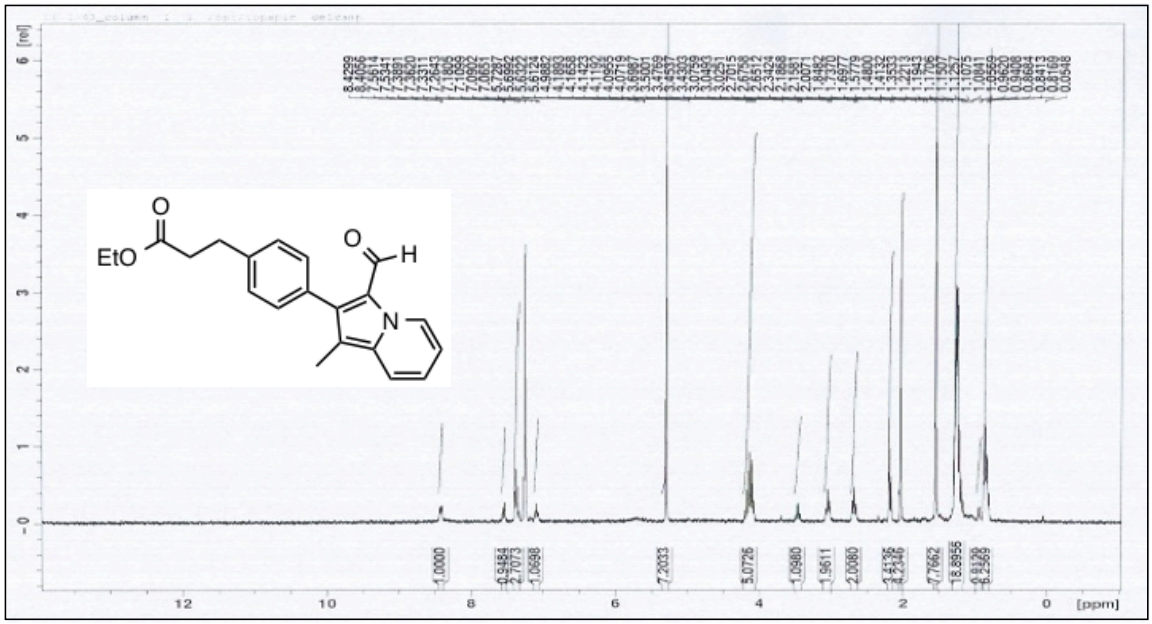

^{1}H NMR: Ethyl (*E*)-3-(4-(3-(2-(4-cyano-5-(dicyanomethylene)-2,2-dimethyl-2,5-dihydrofuran-3-yl)vinyl)-1-methylindolizin-2-yl)phenyl)propanoate (10)

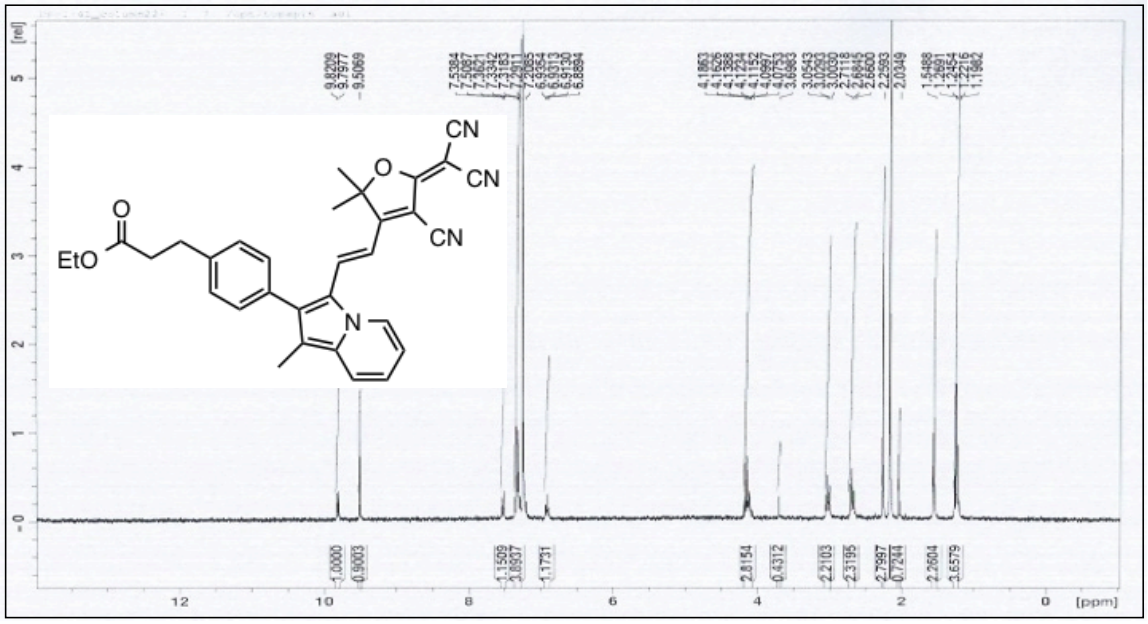

^{1}H NMR: (*E*)-3-(4-(3-(2-(4-cyano-5-(dicyanomethylene)-2,2-dimethyl-2,5-dihydro furan-3-yl)vinyl)-1-methylindolizin-2-yl)phenyl)propanoic acid (DP3)

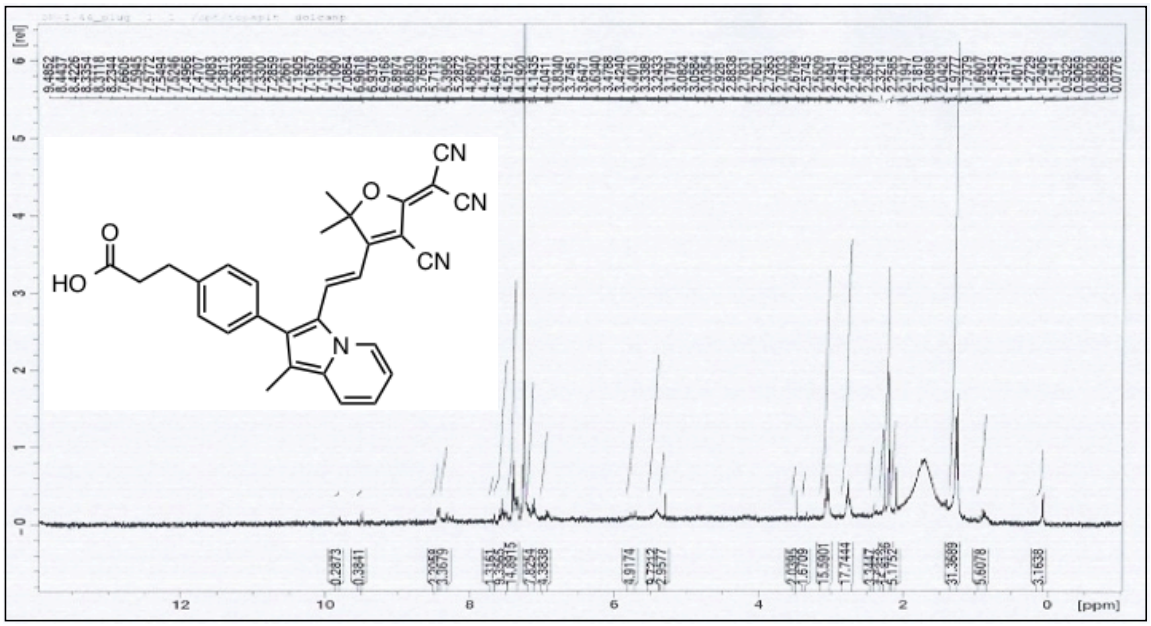

Input Files for DP1 and DP2.

%chk=DP1_tddft.chk
%mem=1000MW
td=(nstates=10) rb3lyp/6-311g(d,p) scrf=check nosymm guess=(huckel,save) geom=connectivity

DP1_tddft

0 1

C	8.12564300	-5.61837300	-0.12713100
C	4.35314900	-0.80336500	0.00330900
C	6.14195200	-4.12521200	-0.18012000
C	8.21799300	-3.42095500	0.94580900
C	7.44750300	-4.33725700	0.17971400
O	5.77359800	3.18260400	-0.11030000
C	6.35226800	4.51025300	-0.17248100
C	5.21494200	5.50565500	-0.07625600
C	6.65120600	2.15728300	-0.12461700
O	7.85101900	2.29157900	-0.18234100
C	1.79512000	-1.11016700	-0.09720700
C	3.17796000	-1.55608800	-0.08716100
S	3.57509400	-3.24124100	-0.17027500
C	5.32120100	-2.97093500	-0.07495800
C	5.54614200	-1.59679600	0.02232600
S	6.97852800	-0.59790200	-0.00792700
C	5.96923600	0.85270000	-0.06326600
C	4.63355400	0.59850400	-0.04346600
C	1.39477400	0.04662200	0.59901200
C	0.07892900	0.47219900	0.60131200
C	-0.91579700	-0.24274400	-0.09623600
C	-0.52230100	-1.40468800	-0.79197500
C	0.79495600	-1.82203900	-0.78760000
C	-3.34009900	11.68006500	-0.52633600
H	-5.80210000	-5.21040100	-0.11793300
H	-6.71960000	-4.28177500	1.08789300
H	-8.78256200	-4.54820200	-0.29734900
H	-7.87502700	-5.48196600	-1.47798400
H	-7.37449000	-7.21614800	0.28113500
H	-8.27790400	-6.28169000	1.45991300
O	9.25807700	-5.89190300	0.18485100
O	7.33254500	-6.48571900	-0.81445000
N	8.82106000	-2.69475000	1.61388100
H	3.89319800	1.38245300	-0.08814700
H	5.65403800	-4.99368000	-0.61030700
H	7.06572800	4.61877500	0.64716800

H	6.90524800	4.60628300	-1.10987400
H	5.61043500	6.52373500	-0.11971600
H	4.51047000	5.37539700	-0.90078900
H	4.67318600	5.38760500	0.86470800
H	2.11931100	0.59097500	1.19178600
H	-0.19635700	1.35249700	1.16708500
H	1.06565100	-2.69981800	-1.36413600
H	7.86800800	-7.28076200	-0.94596300
H	-9.45435100	-7.49314200	-1.09524600
H	-9.84474300	-8.26427400	1.84248900
H	-1.25932600	-1.96589200	-1.35104400
C	-6.66981000	-4.55338700	0.02548300
O	-6.51947200	-3.37312500	-0.76748600
C	-8.22110100	-6.52649600	0.39157000
C	-7.94911900	-5.24932500	-0.41059100
C	-9.51012200	-7.24243100	-0.02831200
H	-10.35760800	-6.55329300	0.07798700
C	-9.79066700	-8.51618200	0.77647600
H	-8.94343800	-9.20442300	0.66980000
C	-11.08016600	-9.22598500	0.35426100
H	-11.24977300	-10.13008900	0.94502500
H	-11.95080600	-8.57585800	0.48508200
H	-11.04320200	-9.51995800	-0.69931300
N	-2.24679300	0.18116800	-0.09500700
C	-4.32746000	-0.51962400	-1.19924800
C	-5.38117500	-1.40745300	-1.33909700
H	-4.28319200	0.36871200	-1.81798100
H	-6.16719900	-1.23300200	-2.06366000
C	-3.31763600	-0.75301200	-0.25561100
C	-3.39524100	-1.89684700	0.53893000
H	-2.62742300	-2.08506200	1.28007500
C	-5.44827900	-2.56286400	-0.54888400
C	-4.44200900	-2.80534300	0.39123500
H	-4.46790200	-3.68323300	1.02205000
C	-2.33923200	3.89569600	-0.50252200
C	-2.01701200	2.55278600	-0.69308700
H	-1.88316100	4.64141700	-1.13910500
H	-1.31529400	2.27773000	-1.47176000
C	-2.57959900	1.55763000	0.10598100
C	-3.49657000	1.92937800	1.09854300
H	-3.94585100	1.16541700	1.72171900
C	-3.83541300	3.25929200	1.28325400
C	-3.25624000	4.25815200	0.48895500
H	-4.54351600	3.55548200	2.04749300
C	-3.11881200	6.60475200	-0.02670600
H	-2.02423200	6.61996700	0.05532200

H	-3.37978600	6.45549900	-1.08252700
C	-3.71471000	7.90090000	0.49850300
H	-4.80601000	7.82822200	0.44659400
H	-3.45526300	7.99898700	1.55782300
C	-3.23069000	9.12965400	-0.27951000
H	-2.13483400	9.17864100	-0.24372100
H	-3.49721400	9.02070700	-1.33857200
C	-3.80935900	10.44583900	0.25213800
H	-4.90531300	10.39633600	0.22494500
H	-3.53661400	10.55967500	1.30904200
H	-2.24456700	11.72618200	-0.50319600
H	-3.61718400	11.56784900	-1.58154100
C	-3.91666000	12.99099300	0.01570100
H	-3.56491500	13.85034800	-0.56133200
H	-5.01031300	12.98899600	-0.02487100
H	-3.62535900	13.14978700	1.05862000
O	-3.64879000	5.53302200	0.75730100

%chk=DP2_tddft.chk
%mem=1000MW
td=(nstates=10) rb3lyp/6-311g(d,p) scrf=check nosymm guess=(huckel,save) geom=connectivity

DP2_tddft

0 1

C	1.94820700	0.40380300	0.03672400
O	1.96316000	4.61958500	-0.38050900
C	7.14888600	-2.84158700	0.08513800
C	-5.27823000	-3.45558400	0.32344400
H	-9.70344200	2.44528700	0.55521000
H	0.78493800	2.30175300	-0.16712800
H	-6.15784600	3.26553600	-0.31636600
C	0.66347900	6.61685500	-0.56855800
C	6.04929400	-1.85070500	0.31573300
H	4.57880700	-3.12180800	-0.43276600
C	-4.65720400	-4.72821200	-0.26930600
H	-7.01692600	-1.44532800	0.88517900
C	6.40902300	-0.72695000	1.10673200
H	-0.57733100	1.01690400	1.26534100
H	-3.02666700	0.99353900	1.29959300
H	-8.66391200	3.66936600	-0.18344300
H	-8.62398000	3.41250800	1.55961600
C	-6.35283200	2.23352100	-0.04188700
C	4.75494100	-2.11884700	-0.04956600

C	-7.62326800	1.87296800	0.41980100
N	-4.53611500	-1.01668000	-0.00882500
C	-3.23863800	-4.28584900	-0.66757400
C	3.12986600	3.94399500	-0.34396200
C	2.06998800	6.05615200	-0.54958800
C	-1.10267000	0.24701400	0.71422500
C	-6.82096000	-0.41766900	0.61018900
C	-8.71248000	2.90269700	0.59388100
C	1.09139100	-0.70052300	0.02542000
C	3.58404300	-1.31695300	0.03485100
C	3.33785700	0.05535200	0.05876200
C	-7.83473200	0.52779300	0.73028600
H	-8.80949400	0.20850300	1.08490900
S	2.02971900	-2.16124100	0.01850800
C	-5.55016300	-0.04668900	0.15309100
C	-5.33548600	1.29830800	-0.18415500
H	-4.37782400	1.60708200	-0.58295500
C	-0.36104000	-0.74227500	0.03990300
C	-2.49045100	0.23464800	0.74580800
C	-3.17290700	-0.79279600	0.08086000
N	6.68978800	0.17049900	1.78001100
C	-2.44756500	-1.81124600	-0.56989800
C	-1.07109500	-1.78699400	-0.59613200
H	-0.52667900	-2.55917700	-1.12959300
S	4.35541300	1.46805800	-0.07004600
C	2.91904800	2.49460600	-0.18029700
C	1.74506000	1.81335700	-0.10076100
O	8.14259200	-2.89694900	0.75213700
O	6.95160000	-3.72426500	-0.93776400
O	4.21855000	4.46060900	-0.43827400
H	2.66407000	6.46026700	0.27300500
H	2.60719100	6.25832000	-1.47894300
H	0.14354400	6.39874300	0.36686600
H	0.70052700	7.70181900	-0.69561600
H	0.08579400	6.19423100	-1.39354400
C	-4.79893300	-2.33475100	-0.62907900
C	-3.40392100	-2.82095700	-1.15773800
H	-5.51740300	-2.19739600	-1.44121800
H	-3.37415300	-2.78308400	-2.25079100
H	-6.36576000	-3.51020900	0.40154800
H	-4.87841900	-3.27083100	1.32581500
H	-4.65942400	-5.56697500	0.42998200
H	-5.22041300	-5.04136400	-1.15551800
H	-2.79054700	-4.92854300	-1.42786100
H	-2.58287900	-4.31004200	0.20741500
H	6.27214700	-3.39161300	-1.53523900